Population exposure to outdoor NO$_2$, black carbon, ultrafine and fine particles over Paris with multi-scale modelling down to the street scale

Soo-Jin Park[1], Lya Lugon[1], Oscar Jacquot[1], Youngseob Kim[1], Alexia Baudic[7], Barbara D'Anna[8], Ludovico Di Antonio[3], Claudia Di Biagio[4], Fabrice Dugay[7], Olivier Favez[5], Véronique Ghersi[7], Aline Gratien[4], Julien Kammer[8], Jean-Eudes Petit[6], Olivier Sanchez[7], Myrto Valari[2], Jérémy Vigneron[7], and Karine Sartelet[1]

[1]CEREA, Ecole des Ponts, EDF R & D, Institut Polytechnique de Paris, IPSL, Marne-la-vallée, France
[2]LMD/IPSL, École Polytechnique, Université Paris Saclay, ENS, PSL Research University, Sorbonne Universités, UPMC Univ, France
[3]Université Paris Est Créteil and Univ. Paris Cité, CNRS, LISA, F-94010 Créteil, France
[4]Université Paris Cité and Univ. Paris Est Créteil, CNRS, LISA, F-75013 Paris, France
[5]INERIS, 60550 Verneuil en Halatte, France
[6]Laboratoire des Sciences du Climat et l'Environnement, CEA/Orme des Merisiers, 91191 Gif-sur-Yvette, France
[7]Airparif, 75004, Paris, France
[8]Aix Marseille Univ, CNRS, LCE, Marseille, France

Correspondence: Karine Sartelet (karine.sartelet@enpc.fr)

Abstract.

This study focuses on mapping the concentrations of pollutants of health interest (NO$_2$, black carbon (BC), PM$_{2.5}$, particle number concentration (PNC)) down to the street scale to represent the population exposure to outdoor concentrations at residences. Simulations are performed over the Greater Paris area with the WRF-CHIMERE/MUNICH/SSH-aerosol chain, using either the top-down inventory EMEP or the bottom-up inventory Airparif with correction of the traffic flow. The concentrations of the pollutants are higher in streets than in the regional-scale urban background, due to the strong influence of road-traffic emissions locally. Model-to-observation comparisons were performed at urban background and traffic stations, and evaluated using two performance criteria from the literature. For BC, harmonized equivalent BC (eBC) concentrations were estimated from concomitant measurements of eBC and elemental carbon. Using the bottom-up inventory with corrected road-traffic flow, the strictest criteria are met for NO$_2$, eBC, PM$_{2.5}$, and PNC. Using the EMEP top-down inventory, the strictest criteria are also met for NO$_2$, eBC, and PM$_{2.5}$, but errors tend to be larger than with the bottom-up inventory for NO$_2$, eBC, and PNC. Using the top-down inventory, the concentrations tend to be lower along the streets than those simulated using the bottom-up inventory, especially for NO$_2$ concentrations, resulting in less urban heterogeneities. The impact of the size-distribution of non-exhaust emissions was analyzed at both regional and local scales, and it is higher in heavy-traffic streets. To assess exposure, a French database detailing the number of inhabitants in each building was used. The population-weighted concentration (PWC) was calculated by weighting populations by the outdoor concentrations to which they are exposed at the precise location of their home. An exposure scaling factor (ESF) was determined for each pollutant to estimate the ratio needed to correct urban back-

ground concentrations in order to assess exposure. The average ESF in Paris and Paris Ring Road is higher than 1 for NO_2, eBC, $PM_{2.5}$, PNC, because the concentrations simulated at the local scale in streets are higher than those modelled at the regional scale. It indicates that the Parisian population exposure is under-estimated using regional-scale concentrations. Although this underestimation is low for $PM_{2.5}$, with an ESF of 1.04, it is very high for NO_2 (1.26), eBC (between 1.22 and 1.24), and PNC (1.12). This shows that urban heterogeneities are important to be considered in order to represent the population exposure to NO_2, eBC, and PNC, but less so for $PM_{2.5}$.

Keywords: multi-scale modelling; population exposure; exposure scaling factor; bottom-up emission inventory; particle number concentration

1   Introduction

In metropolises, characterised by densely populated and extensively developed areas, air pollution remains a major concern due to the presence of numerous emission sources, such as traffic, energy consumption, solvents, industrial activities. Traffic emissions receive particular attention because of their influence on local concentrations, with an impact of both exhaust and non-exhaust emissions (Fu et al., 2020; Jereb et al., 2021; Holnicki et al., 2021; Sarica et al., 2023). Environmental regulations aim to reduce key air pollutant concentrations, such as NO_2, O_3, and fine particulate matter ($PM_{2.5}$). Although a large part of the health impacts are attributed to particles (Southerland et al., 2022), the health effects associated with different particle compounds and different particle size can vary considerably (Park et al., 2018; WHO, 2021; Haddad et al., 2024). In particular, black carbon (BC) and ultrafine particles (UFP, defined by particles with diameter lower than 0.1 μm) are considered "priority" emerging pollutants (WHO, 2021; Goobie et al., 2024) that need to be better characterized, as stated in the recent European air-quality directive 2024/2881/CE. Long-term exposure to ultrafine particles is associated with increased mortality (Li et al., 2023b; Schwarz et al., 2023), while BC has been linked to adverse health effects, especially in urban areas (Lequy et al., 2021; Bouma et al., 2023; Kamińska et al., 2023). Whereas fine particles are best characterized by their mass concentrations ($PM_{2.5}$), the mass of UFP is low compared to that of fine particles. Hence, UFPs are best characterized by their particle number concentrations (PNC) (Kwon et al., 2020; Trechera et al., 2023), contributing to about 80-90% of the PNC over urban areas (Dall'Osto et al., 2013; Abbou et al., 2024).

Although modelling is often use to assess the effect of emissions and policies to improve air quality in cities (Mao et al., 2005; Yuan et al., 2014; Kuklinska et al., 2015; Selmi et al., 2016; Andre et al., 2020; Lugon et al., 2022), assessments on BC and UFP concentrations are not frequently evaluated, because they are not regulated, nor measured routinely in cities and difficult to model. Difficulties to model BC are partly linked to differences between elemental carbon and black carbon (Savadkoohi et al., 2023), contributing to large model/measurement discrepancies (Lugon et al., 2021b). However, recommendations for assessing BC concentrations were recently provided by Savadkoohi et al. (2024). The PNC are even more difficult to model, because of the lack of emission inventories and the rapid transformations of the ultrafine particles involved (Kukkonen et al., 2016). The difficulties to model BC and PNC might also partly be linked to the strong influence of traffic emissions on their concentrations (Andre et al., 2020; Jia et al., 2021; Lugon et al., 2022; Li et al., 2023a; Trechera et al., 2023). Traffic emissions are highly

spatially and temporally variable in cities, and their variability is not easily reproduced in emission inventories. Those are usually built using either top-down or bottom-up approaches (Guevara et al., 2016). Bottom-up approaches use detailed spatial and temporal information for each activity sector, e.g., the number of vehicles for traffic emissions, while top-down approaches use information defined at larger scales (regional or national), which are spatialized using specific data, such as population data.

55 Significant discrepancies may exist between emission inventories using these two approaches (Guevara et al., 2016; Lopez-Aparicio et al., 2017), especially for traffic emissions (Lopez-Aparicio et al., 2017) and non-exhaust emissions from tire, brake, and road wear (Piscitello et al., 2021; Tomar et al., 2022). Emission inventories for UFP only exist for top-down inventories (Kulmala et al., 2011; Zhong et al., 2023). Sartelet et al. (2022) recently provided a methodology to estimate UFP emissions from any emission inventories of PM, making it possible to use either bottom-up or top-down emission inventories.

60 Population exposure to outdoor concentrations at residences is commonly used as a proxy for exposure in epidemiological studies (Hoek et al., 2024), or it is used as an input when estimating multi-environment exposure (Karl et al., 2019; Valari et al., 2020; Elessa Etuman et al., 2024). In epidemiological studies, exposure to outdoor concentrations at residence is often estimated using Land-Use Regression models (Ma et al., 2024), which are usually based on linear regressions using land-use predictor variables and data from fixed monitoring stations and passive sampling. Regional-scale models (chemical transport 65 models with a spatial resolution often coarser than a few km^2) are sometimes used (Ostro et al., 2015; Adélaïde et al., 2021), leading to simulated fine PM concentrations much lower than those simulated using LUR models (Lequy et al., 2022). Their use is limited, because they are not able to represent the urban heterogeneities, e.g. gradients between street and background concentrations.

Multi-scale models, i.e. a combination of regional and local-scale models (Kwak et al., 2015; Lee and Kwak, 2020; Park 70 et al., 2021; Lugon et al., 2022; Lin et al., 2023; Wang et al., 2023b; Strömberg et al., 2023), do represent urban heterogeneities, but they are often not able to represent the PM composition and the UFP, or their application is limited to a city district. To represent an entire city, chemical-transport models are often coupled with a simple representation of local dispersion (Hood et al., 2018; Karl et al., 2019; Lugon et al., 2022; Maison et al., 2024b) or with subgrid statistical approaches (Valari and Menut, 2010; Squarcioni et al., 2024). However, only a few studies model BC (Lugon et al., 2021b) and PNC (Zhong et al., 75 2023; Ketzel et al., 2021) concentrations down to the street scale. To model PNC, the main difficulty lies in the evaluation of atmospheric transformations (Kukkonen et al., 2016; Strömberg et al., 2023), and there is to our knowledge no multi-scale model currently available to represent PNC over a whole city from the urban background down to the street scale taking into account aerosol dynamics. To simulate gas and particle concentrations over cities from the regional down to the local scale taking into account chemistry and aerosol dynamics, the chemical module SSH-aerosol (Sartelet et al., 2020) has been coupled 80 with air quality models at the street and regional scales: the street-network Model of Urban Network Intersecting Canyons and Highways (MUNICH) (Kim et al., 2018, 2022) and the regional-scale models Polair3D (Lugon et al., 2021a, 2022; Sarica et al., 2023; Sartelet et al., 2024) and CHIMERE (Maison et al., 2024b; Squarcioni et al., 2024). The coupled multi-scale systems represent concentrations from the regional down to the street scales, taking into account all emission sources and secondary particle formation at all scales consistently (Lugon et al., 2022; Sartelet et al., 2024). Although extensive comparisons to 85 observations were performed at the regional and local scales for NO$_2$, PM$_{2.5}$, and PM$_{10}$ (Sartelet et al., 2018; Lugon et al.,

2022; Kim et al., 2022; Sarica et al., 2023), urban multi-scale modelling evaluation of BC and PNC at both regional and local scales is still missing.

This study aims to define a methodology for simulating multi-pollutant concentrations, including BC and PNC, down to the street scale over Paris, and to estimate the influence of spatial heterogeneities on the population exposure to outdoor concentrations at residences. Using detailed population data per building, an indicator is presented to assess how much regional modelling underestimates population exposure for different pollutants. It varies depending on the pollutants and in particular on their urban variability. Section 2 describes the model and simulation setup, including the PN emissions (section 2.2.1), as well as the relative contributions of non-traffic, exhaust, non-exhaust, and other traffic emissions (Section 2.2.2). Section 2.2.3 details the setup for a sensitivity simulation related to the size distribution of non-exhaust emissions. The model is evaluated at background and traffic stations in section 3, and the influence of the emission inventory and the size distribution of non-exhaust emissions is assessed. In section 4, using detailed population data at building level, a scaling exposure factor is determined to estimate outdoor population exposure for the city of Paris using modelled regional-scale concentrations.

2 Material and methods

The different abbreviations used throughout this paper are summarized in Table 1.

Table 1. List of abbreviations

	Nomenclature
BC	Black carbon
eBC	Equivalent Black Carbon
PNC	Particle Number Concentration
LUR	Land-Use Regression
CTM	Chemical Transport Model
UFP	UltraFine Particles
REF	Reference simulation
SEN	Sensitivity simulation
PWC	Population Weighted Concentration
ESF	Exposure Scaling Factor

2.1 Model description and simulation setup

Simulations are performed with WRF-CHIMERE/MUNICH/SSH-aerosol from 01 UTC on 1 June 2022 to 23 UTC on 31 July 2022, corresponding to a period with specific PNC and BC measurements performed over Paris, as detailed in section 2.4. The setting is the same as in Maison et al. (2024b), and it is summarized here.

The CHIMERE chemistry-transport model (v2020r1) (Menut et al., 2021) is applied over Greater Paris (Île-de-France) to compute atmospheric concentrations of gas-phase and aerosol species considering transport (advection and mixing), deposition, emissions, chemistry and aerosol dynamics. The chemical scheme used is MELCHIOR2 modified to represent the formation of organic condensables as described in SSH-aerosol v1.3 (Sartelet et al., 2020), which is used for aerosol dynamics (coagulation and condensation/evaporation). The SSH-aerosol model integrates three modules: SCRAM (Size-Composition Resolved Aerosol Model), which addresses the dynamic evolution of aerosols; SOAP (Secondary Organic Aerosol Processor) for gas/particle partitioning of organic compounds; and H^2O (Hydrophobic/Hydrophilic Organics) for the formation of condensable organic compounds. The particle size distribution is discretized in 10 sections of diameters between 0.01 and 10 μm (Appendix A). The CHIMERE model is coupled with the meteorological model Weather and Research Forecasting (WRF) (Powers et al., 2017), which was used to compute the meteorological fields needed in the simulation. Here, no feedback interactions are considered between concentrations and meteorological fields, with a one-way coupling approach.

For a fine description of the urban background concentrations over Paris, a fine spatial resolution of 1 km^2 is used over Greater Paris (IDF1 domain, Figure 1). Boundary conditions are obtained by simulating three nested domains: the intermediate domain covers the north-west of France with a horizontal resolution of 3 km x 3 km (IDF3 domain), and the outermost domain covers France and western Europe with a horizontal resolution of 9 km x 9 km (FRA9 domain, Figure 1). CAMS (Copernicus Atmosphere Monitoring Service) reanalysis (Inness et al., 2019) are used as boundary conditions of this outermost domain. The model setup is the same as in Maison et al. (2024a).

In WRF, the vertical is discretized with 33 levels ranging from 0 to 20 km of altitude. The single-layer urban canopy model (UCM) (Kusaka et al., 2001) is used in the domains IDF3 and IDF1 in order to improve the representation of meteorological fields in urban areas, using the CORINE land cover database (available in 10.2909/71c95a07-e296-44fc-b22b-415f42acfdf0), which classes the urban areas in three sub-categories (commercial areas, high intensity residential and low-intensity residential areas). More details about WRF simulations setup are available in Maison et al. (2024a).

In CHIMERE, the vertical discretization is based on 15 isobaric vertical levels, from 998 hPa to 500 hPa, resulting in average layer heights ranging from 17 m near the ground to 1050 m at high altitudes. The land-use database GLOBCOVER (Arino et al., 2007), with 300 m spatial resolution, is used to compute pollutant deposition and biogenic emissions, which are estimated following MEGANv2.1 (Guenther et al., 2012).

The WRF-CHIMERE/SSH-aerosol model is one-way coupled to the street-network model MUNICH (Kim et al., 2022). SSH-aerosol is used both in CHIMERE and MUNICH, in order to represent consistently chemical and aerosol species at all scales. In MUNICH, dry and wet depositions are considered through the parameterizations detailed in Kim et al. (2022). The street network contains the 4655 main streets of Paris (Figure 1). Traffic emissions are diluted in each street volume, which depends on street height, length, and width. Gas and particle compounds are advected from one street to another, depending on the wind direction, and the vertical transfer of pollutants between the urban background and streets depends on atmospheric stability, which is determined depending on the Monin-Obukhov length (LMO), Planetary boundary layer (PBL) height, and the standard deviations of wind velocity.
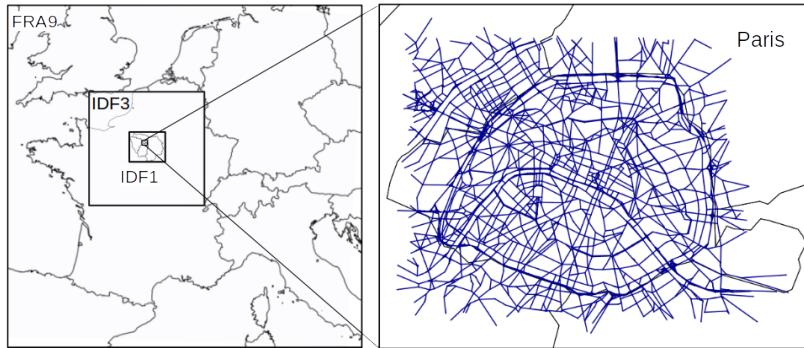
Figure 1. Domains for the regional- and local-scale simulations. The blue lines on the right panel represent the street segments used in the local-scale simulation.

MUNICH v2.2 is employed with an updated calculation of the LMO to better represent the vertical transfer of pollutants between the streets and the background. In previous studies (Kim et al., 2022; Lugon et al., 2022; Sarica et al., 2023), the LMO was parameterized following Musson-Genon (1992) derived from evaporation and sensible heat fluxes at the surface. Using this parameterization, for all street segments during the period of simulation, 93.8% of atmospheric conditions are unstable, 6.2% are stable, and nearly 0% are neutral. This study uses instead the LMO parameterization of Soulhac et al. (2011), which calculates the sensible heat flux by deriving it from net radiation, latent heat flux, and diffusive heat flux toward the ground. As a result, there are less frequent unstable but more neutral conditions: 68.8% of the conditions are unstable, 7.6% are stable, and 23.6% are neutral. Using both parameterizations, stable and neutral conditions appear predominantly during nighttime. However, using the parameterization of Soulhac et al. (2011) leads to much better comparisons to concentration measurements than the parameterization of Musson-Genon (1992), indicating that stable and neutral conditions may not well be represented during summer in cities with the parameterization of Musson-Genon (1992).

For aerosol dynamics, coagulation and condensation of sulfuric acid and low-volatile organic compounds are resolved simultaneously and dynamically for all particle sizes. The Kelvin effect is taken into account when simulating condensation/evaporation of semi-volatile compounds, as described in Zhu et al. (2016). As condensation/evaporation is resolved using a Lagrangian approach, the section diameters may evolve and the Euler-coupled algorithm is used to redistribute the particle mass and number concentrations into the sections of fixed size classes (Sartelet et al., 2020). Because the first diameter is relatively high (10 nm), if the diameter of the particles of the first section goes below 10 nm, then the mass of those particles is allocated to the first section.

Using a one-way coupling approach, the regional-scale and local-scale simulations are performed sequentially. For the regional scale, the two-month simulation using WRF-CHIMERE models requires approximately 11520 processor hours (192 processors over 60 hours). The local scale simulations are less expensive, and the two-month simulation with the MUNICH model requires around 7680 processor hours (64 processors over 120 hours) to simulate the street concentrations in the Parisian street-network composed of 4655 streets.

2.2 Anthropogenic emissions

In the regional-scale modelling with CHIMERE, the top-down 2020 anthropogenic emission inventory of EMEP (European Monitoring and Evaluation Program) of spatial resolution 0.1° x 0.1° is used for the larger-scale simulations over Western Europe (FRA9 domain) and the North-west of France (IDF3 domain). Over Greater Paris, two different simulations are performed: one with the EMEP inventory, labelled as "EMEP" in the following, and one with the bottom-up inventory of Airparif, the air-quality monitoring network for the Greater Paris area, labelled as "REF" in the following. The spatial resolution of the Airparif inventory is 1 km x 1 km, except for traffic emissions with a finer resolution down to the street level. Note that in the REF simulation, even though the Airparif bottom-up inventory is used over Greater Paris, the EMEP inventory is used for the cells outside the Greater Paris area that are not covered by the Airparif inventory, i.e. exclusively on the edge of the Greater Paris area. In the street-network model MUNICH, only the Airparif inventory is used, because there is no downscaling available for EMEP emissions down to streets.

The bottom-up inventory corresponds to the 2019 Airparif inventory for all activity sectors except for traffic, which is specific to the summer 2022. It is calculated using the traffic emissions model HEAVEN (https://www.airparif.asso.fr/heaven-emissions-du-trafic-en-temps-reel). The strength of this system is to use a traffic model that is corrected from traffic count data in near real time. Non-traffic and traffic emissions are detailed in Appendix B (sections B1 and B2, respectively). For consistency between traffic emissions in the streets and at the urban scale, street-scale traffic emissions are aggregated and assigned to the corresponding grids in the CHIMERE model (Figure 2 a and c). The emissions of NO_2 and BC are higher along the main roads and motorways. In Paris, emissions are higher on the Paris Ring Road than in the city center. Section 2.2.1 details the algorithm to represent PN emissions, section 2.2.3 details the size distribution of non-exhaust emissions, and the sensitivity simulation on its representation (labelled as "SEN").

2.2.1 PN emissions

The emission inventories provide estimations of particle matter in different sizes for the different activity sectors. Here, the non-traffic emission inventory provides emission data for $PM_{2.5}$ and PM_{10}, while the traffic emission inventory provides emission data for $PM_{2.5}$, PM_{10} and PM_1. The particle emissions are distributed in the modelled particle size sections following Sartelet et al. (2022). Emissions of particles in the range $PM_{0.1}$-PM_1 and $PM_{0.01}$-$PM_{0.1}$ are estimated using the PM_1/$PM_{2.5}$ and $PM_{0.1}$/PM_1 ratios given in Sartelet et al. (2022) (Table A1) for each activity sector.

Emissions in each of the size ranges: $PM_{0.01}$-$PM_{0.1}$, $PM_{0.1}$-PM_1, and PM_1-$PM_{2.5}$ are distributed among the model size sections within that range using the formula:

$$M_i = M \frac{d_i^{3/2} - d_{i-1}^{3/2}}{d_n^{3/2} - d_0^{3/2}} \quad (1)$$

where M is the mass concentration to be distributed, i is the size section of bound diameters d_{i-1}-d_i included in the size range of bound diameters d_0-d_n. This formula, which is set out in Appendix A, allows the conservation of both mass and number during the discretisation. The detailed factors obtained with this formula for each size section are presented in Table A1.
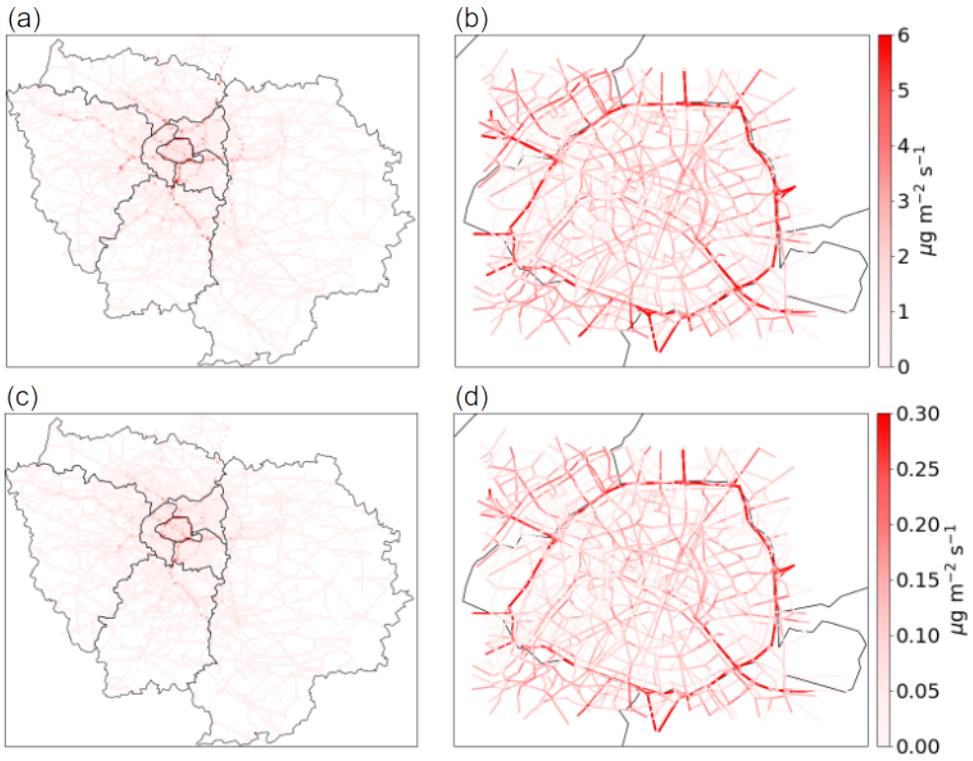
Figure 2. Regional (left panels) and street (right panels) traffic emissions of NO$_2$ [(a) and (b)] and BC [(c) and (d)] averaged from June to July 2022

2.2.2 Emission sources of NOx, BC, PM, and PNC

The distribution between traffic (exhaust vehicular road, non-exhaust vehicular road, non-road/other traffic) and non-traffic emissions for NOx, BC, PM, and PNC over Greater Paris is shown in Figure 3, and over Paris in Figure C1. Non-traffic emissions refer to all emissions excluding traffic emissions (exhaust vehicular road emissions, non-exhaust vehicular road emissions, non-road/other traffic emissions). Exhaust emissions are produced from the combustion processes associated with road traffic emissions, while non-exhaust emissions include road-traffic emissions resulting from road wear, tire wear, and brake wear. Other-traffic emissions encompass emissions from ships and aircraft. Over Greater Paris, the majority of NOx emissions originated from road traffic sources (65.8%). Amongst non-road traffic sources, shipping, railways, and aviation contribute to a significant proportion (24.9%) of NOx emissions. PM$_{2.5}$ emissions are mostly from non-traffic sources (over 69% of PM emissions), while road traffic contributes only to about 30.5% of emissions. Note that non-exhaust emissions represent a larger percentage of PM$_{2.5}$ than exhaust emissions (22.2% vs 8.3%). Concerning BC emissions, the influence of road traffic is larger than that of PM$_{2.5}$ emissions (about 46.1% of BC emissions), with a larger contribution of exhaust than
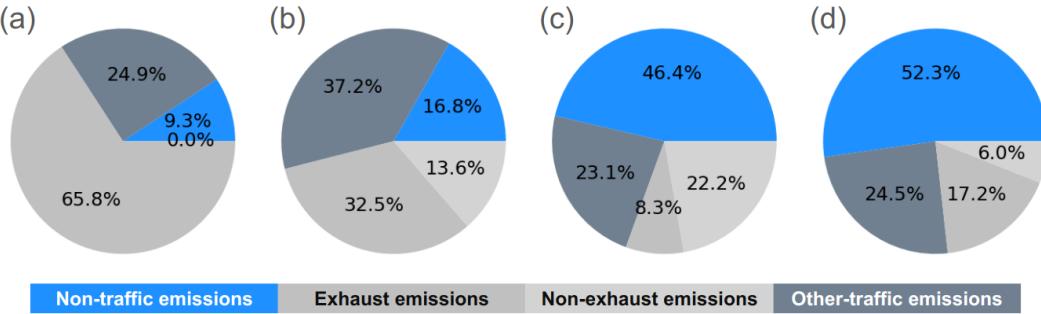
Figure 3. Distribution between vehicular road traffic (exhaust and non-exhaust), non-road/other traffic and non-traffic emissions for NOx (a), BC (b), PM$_{2.5}$ (c), and PNC (d) in Greater Paris.

non-exhaust emissions (32.5% vs 13.6%). Concerning PN emissions, non-traffic sources constitute almost half of the emissions (52.3%), with a contribution of road traffic to about 17.2%, and a strong contribution of non-road traffic sources (24.5%).

2.2.3 Sensitivity to non-exhaust emissions size distribution

Non-exhaust traffic emissions, such as tire wear, brake, and road wear, have large uncertainties (Lugon et al., 2021b), and their contribution to particle emissions is also large. Section 2.2.2 shows that non-exhaust emissions (22.2%) contribute more to traffic PM emissions than exhaust emissions (8.3%). In the emission inventory, the non-exhaust emissions of particles are provided for PM$_{10}$. Emissions of PM$_{2.5}$ and PM$_1$ are estimated using a PM$_1$/PM$_{2.5}$ ratio and a PM$_{2.5}$/PM$_{10}$ ratio. A sensitivity simulation "SEN" is set-up to evaluate the impact of the choices made in this size distribution of non-exhaust emissions. In the reference simulation, the PM$_1$/PM$_{2.5}$ ratio and PM$_{2.5}$/PM$_{10}$ ratio for non-exhaust emissions are obtained from EMEP guidelines for the different types of vehicles (Ntziachristos, 2016). In the SEN scenario, the PM$_{2.5}$/PM$_{10}$ ratios are modified to be those of the NORTRIP model (Denby et al., 2013). The size distribution employed in REF and SEN simulations is detailed in Table 2.

Table 2. PM$_{2.5}$/PM$_{10}$ ratios of particles emitted from non-exhaust traffic sources in the REF and SEN simulations.

	Tire	Brake	Road
REF	0.70	0.40	0.54
SEN	0.10	0.63	0.04

Non-exhaust emissions are almost equally distributed between PM$_{2.5}$ and PM$_{10}$ in the REF simulation (PM$_{2.5}$/PM$_{10}$ = 0.53), while the proportion of non-exhaust emissions in PM$_{2.5}$ is lower in the SEN simulation (PM$_{2.5}$/PM$_{10}$ = 0.28). As the NORTRIP model has no PM$_1$/PM$_{2.5}$ ratio for non-exhaust emissions, no modifications are made in the PM$_1$/PM$_{2.5}$ ratios in the SEN simulation. The proportion of PM$_1$ is low in both REF and SEN (PM$_1$/PM$_{10}$ $\simeq$ 0.07).

2.3 Calculation of population exposure

The population exposure to outdoor concentrations may be calculated using regional-scale modelling, potentially underestimating the exposure. To estimate how well the population exposure is represented using regional-scale modelling for the different pollutants, the population-weighted concentration (PWC) and exposure scaling factor (ESF) are calculated for Paris using the multi-scale concentrations and the population data from the MAJIC database (Létinois, 2014). The 'MAJIC' spatialization method provides a very detailed description of the population on a local scale. More specifically, it uses data on residential premises from the MAJIC property database issued by the French Public Finance Department (DGFiP). This data is cross-referenced with IGN spatial databases (BD PARCELLAIRE https://geoservices.ign.fr/bdparcellaire and BD TOPO, https://geoservices.ign.fr/documentation/donnees/vecteur/bdtopo) and population statistics from the National Institute of Statistics and Economic Studies (INSEE) to estimate the number of inhabitants in each building.

To locate the buildings in the street network, streets are considered as rectangles of known four extremity coordinates, and buildings are located into the street segments by comparing their mean coordinates with those of streets. Because of uncertainty about street widths, buildings within a perimeter on each side of the street are integrated into the street segment (Figure C2).

Among the 109,152 buildings of Paris, 66.9% are integrated into street segments. This corresponds to 44.4% of the population living near main streets, and the remaining 55.6% residing away from main streets.

PWC is calculated by weighting populations based on the concentrations to which they are exposed at the precise location of their home. People living in a building on the main street are assigned to that street concentration. People living in buildings away from busy streets are assigned to urban background concentrations.

$$PWC_{I,J} = \frac{(POP \cdot C)_{I,J}^{st} + POP_{I,J}^{bg} \cdot C_{I,J}^{bg}}{POP_{I,J}^{st} + POP_{I,J}^{bg}} \tag{2}$$

with

$$(POP \cdot C)_{I,J}^{st} = \sum_{s,building \in I,J} POP^{building,s} \cdot C^{st}(s) \tag{3}$$

where I and J are the grid points of the regional-scale model, C^{st} and C^{bg} are the street and urban background concentrations, respectively. $POP^{building,s}$ is the population living in the street segment. $POP_{I,J}^{st}$ is the population living near main streets in the grid cell I, J, POP^{bg} is the population not living near main streets, which is assumed to be exposed to urban background concentrations.

2.4 Measurements

The simulated concentrations are compared to measurements at background and traffic stations (Figure C3). Concerning the measurements operated by Airparif, NO$_2$ and PM$_{2.5}$ are routinely monitored at 21 and 8 stations, respectively. BC was monitored at 4 stations using a dual spot aethalometer (MAGE Sci. model AE33 M8060, using the optical wavelengths 880 nm for eBC analysis) with a PM$_{2.5}$ size cut off, and PNC was monitored using a Mobility Particle Size Spectrometer (MPSS)

for particles of diameters between 5 nm and 385 nm at two stations: Châtelet-les-Halles (PA01H), which is an urban background station located in the center of Paris, and BP-EST, which is next to the very busy Ring road of Paris. At the PA01H station, EC was also measured using filter measurements. It is analysed according to a thermo-optical method (Instrument : Laboratory OCEC Carbon Aerosol Analyser, SUNSET), which meets the EUSAAR2 protocol. The concomittant EC and eBC measurements allow the determination of the harmonization factor suggested by Savadkoohi et al. (2024).

Air-quality models represent the mass concentrations of elemental carbon (EC). They may differ from BC concentrations (Savadkoohi et al., 2023), which are inferred from optical measurements using aethalometers (Drinovec et al., 2015). Equivalent BC (eBC) is then defined as the mass concentration of BC as indirectly determined by light absorption techniques (Savadkoohi et al., 2024). A harmonization of BC measurements is needed to allow for direct comparisons between measured eBC and modeled EC concentrations (Savadkoohi et al., 2024). The harmonization factor was calculated as the ratio of eBC and EC. Between 9 and 22 June 2022, at the PA01H station where both EC and eBC data are available, the daily harmonization factor ranges from 1.34 to 2.26 with an average equal to 1.79 (Figure C4). This average harmonization factor is used to correct the eBC measured concentrations at all stations and all times. Note that the average harmonization factor (1.79) is similar to the harmonization factor of 1.76 proposed by Savadkoohi et al. (2023).

Comparisons are also performed at the SIRTA site (Site Instrumental de Recherche par Télédétection Atmosphérique), an atmospheric observatory located 20 km south-west of Paris which is integrated in the ACTRIS European Research Infrastructure Consortium (https://www.actris.eu) (Haeffelin et al., 2005). In summer 2022, two other monitoring stations were operated inside Paris: the Paris Rive Gauche (PRG) urban background station and the Hôtel de Ville (HdV) traffic station. The PRG site, located on the 7th floor of the Lamark B building of Université Paris Cité (30 m above ground layer), in the south-east side of the city, was set up as part of the ACROSS (Atmospheric ChemistRy Of the Suburban foreSt) campaign (Cantrell and Michoud, 2022). Air was taken from a common certified PM_1 sampling head located on the roof of the building at about 30 m high above the ground level. A copper tube of 7 mm inner diameter and 10 m length connected the PM_1 head to a 4–way stainless steel flow splitter (TSI) located in the measuring room that dispatched the airflow to different instruments. The Paris HdV station was setup as part of the sTREEt (Impact of sTress on uRban trEEs and on city air quality) project (Maison et al., 2024a). It overlooks the quays of the Seine, which is a major road traffic artery. The eBC was monitored with an AE33 at all stations (MAGE Sci. model AE33 M8060, using the optical wavelengths 880 nm), with a $PM_{2.5}$ size cut off at SIRTA and HdV, and a with a PM_1 size cut off at PRG. The PNC was monitored with an SMPS for particles of diameters between 9 nm and 836 nm at SIRTA, and between 23 nm and 1 μm at PRG. A "nano" SMPS, measuring in the range 8 nm - 64 nm was used at PRG to supplement measurements for diameters between 8 and 23 nm. Note that for comparison between simulated and measured concentrations, only particles of diameters larger than 10 nm are considered. The PNC measurements at PRG and SIRTA were performed for shorter periods than the Aiparif measurements at PA01: from 17 June to 11 July at PRG, and from 15 June to 17 July at SIRTA.

3 Evaluation of model performances

Model-to-observation comparisons are performed over urban background stations to evaluate the regional-scale concentrations simulated with CHIMERE, and over traffic stations to evaluate the street-scale concentrations simulated with MUNICH. Model performances are evaluated based on statistical indicators, including the fractional bias (FB), geometric mean bias (MG), normalised mean square error (NMSE), geometric variance (VG), normalised absolute difference (NAD), and the fraction of predictions within a factor of 2 of observations (FAC2), as described in Section D. Following Hanna and Chang (2012) and Herring and Huq (2018), two different acceptable criteria are considered: (i) a strict performance criteria, with |FB| < 0.3, 0.7 < MG < 1.3, NMSE < 3, VG < 1.6, NAD < 0.3, and FAC2 > 0.5; and (ii) a less strict performance criteria, acceptable for urban areas, with |FB| < 0.67, NMSE < 6, NAD < 0.5, and FAC2 > 0.3. For evaluating PNC, many studies (Olin et al., 2022; Patoulias and Pandis, 2022a; Sartelet et al., 2022) rather used the NMB, which is the normalized mean bias, and NME the normalized mean error.

3.1 Background concentrations

The average statistical indicators obtained in each CHIMERE simulation (REF, SEN, and EMEP simulations) are presented in Table 3. The most strict criteria are also met for all pollutants in the simulations using the bottom-up emission inventory (REF and SEN simulations). In the EMEP simulation, concentrations tend to be over-estimated for all pollutants, and the NO_2, eBC, $PM_{2.5}$, and PNC concentrations are higher than those in the REF and SEN simulations (Figure C5) due to relatively high emissions compared to bottom-up traffic emissions. For NO_2, eBC, $PM_{2.5}$, and PNC, the emission ratios of EMEP to bottom-up emissions are 1.2, 1.72, 1.12, and 1.53 in Greater Paris, respectively.

As the sensitivity simulation differs from the reference one by the size distribution of non-exhaust emissions between $PM_{2.5}$ and PM_{10}, the differences between the REF and SEN simulations are negligible for all pollutants. They are also very low for $PM_{2.5}$, suggesting that the choice of the EMEP or NORTRIP size distribution of non-exhaust traffic emissions has a low influence at the regional scale. The differences are the highest for eBC, as the speciation of non-exhaust emissions differs for $PM_{2.5}$ and PM_{10} (see Table B1).

The simulation performance regarding PNC is also evaluated based on NMB and NME, following Olin et al. (2022), Patoulias and Pandis (2022a), and Sartelet et al. (2022). The concentrations simulated with the bottom-up inventory presented very low bias NMB (between -0.3% for REF and -0.7% for SEN) and low NME (24%). Using the EMEP top-down inventory, the NMB and NME are higher (27% and 37% respectively). These values are low compared to studies in the literature. For example, for particles of diameters larger than 0.01 μm, NME values range between 36% and 79% (Sartelet et al., 2022), 63% (Patoulias and Pandis, 2022b), 94% (Olin et al., 2022), and Ketzel et al. (2021) reported an NMB of 151%.

Figure 4 shows the model-to-observation comparison of PNC for different size sections. All simulations reproduced well the size distribution of PNC, although the concentrations are overestimated in the first size section, between 10 and 20 nm. This overestimation may be partly due to the redistribution algorithm, where the mass of particles whose diameter becomes lower than 10 nm during the simulation is assigned to the first size section, as detailed in section 2.1.

Table 3. Statistical indicators for NO_2, eBC, $PM_{2.5}$, and PNC simulated at the background stations in the REF, SEN, and EMEP simulations. The average simulated and observed concentrations are in $\mu g\ m^{-3}$ for NO_2, eBC, $PM_{2.5}$, and in $\#\ cm^{-3}$ for PNC. Bold values do not respect the most strict performance criteria.

	NO_2		eBC			$PM_{2.5}$			PN		
	REF/SEN	EMEP	REF	SEN	EMEP	REF	SEN	EMEP	REF	SEN	EMEP
Number of stations	21		4			8			3		
Observation	14.97		0.44			7.20			8176		
Simulation	14.74	17.50	0.36	0.35	0.54	6.76	6.67	7.29	8173	8138	10610
FB	-0.03	0.15	-0.15	-0.19	0.24	-0.05	-0.06	0.03	-0.01	-0.01	0.23
MG	1.04	1.24	0.97	0.94	0.82	1.04	1.02	1.11	1.05	1.05	**1.34**
NMSE	0.21	0.20	0.35	0.38	0.28	0.20	0.20	0.18	0.10	0.10	0.16
VG	1.21	1.24	1.30	1.32	0.80	1.17	1.18	1.18	1.18	1.18	1.28
NAD	0.17	0.17	0.21	0.22	0.20	0.16	0.16	0.15	0.12	0.12	0.16
FAC2	0.90	0.87	0.80	0.80	0.79	0.92	0.92	0.91	0.98	0.98	0.89
NMB (%)	0.1	19	-10	-13	34	-2	-3	6	-0	-1	27
NME (%)	33.5	38	39	40	50	31	31	32	24	24	37

The better performance of REF and SEN simulations compared to EMEP is more visible in dense-urban areas, probably because the share of traffic is more important than in less dense areas and traffic emissions are better represented thanks to the correction of traffic emissions based on vehicle counting loops (see Section 2.1). Figure 5 shows the daily time series for the NO_2, eBC, $PM_{2.5}$, and PNC in the city center (PA01H station) measured and simulated with the three CHIMERE simulations. Especially for eBC, the temporal evolution of pollutants is better represented with the REF and SEN simulations than the EMEP one, enhancing the importance of a precise traffic emission inventory. Large concentration peaks of $PM_{2.5}$ and eBC are observed at all stations on 19 July. They could explained by forest fires in the South West of France (Menut et al., 2023). Apart from this peak, in both the REF and SEN simulations, the daily variations of NO_2, eBC, $PM_{2.5}$, and PNC are well simulated. As observed for the statistical indicators, the effect of changing the size distribution of non-exhaust emissions (SEN simulation) is low on eBC, $PM_{2.5}$, and PNC at urban background stations, and using the EMEP emission inventory leads to an overestimation of concentrations.

3.2 Street concentrations

Table 4 summarizes the statistical indicators for NO_2, eBC, and $PM_{2.5}$ concentrations at the traffic stations. The strict performance criteria are met for all pollutants: NO_2, eBC, and $PM_{2.5}$ concentrations, for both the REF and SEN simulations.

Figure 6 shows the daily temporal variations of the concentrations of NO_2, eBC, and $PM_{2.5}$ at two different traffic stations: HAUSS, representing a street in the city center, and BP_EST, representing a heavy-traffic road. As expected, the concentrations are largely underestimated by the regional-scale concentrations simulated with CHIMERE. The daily variations of the street
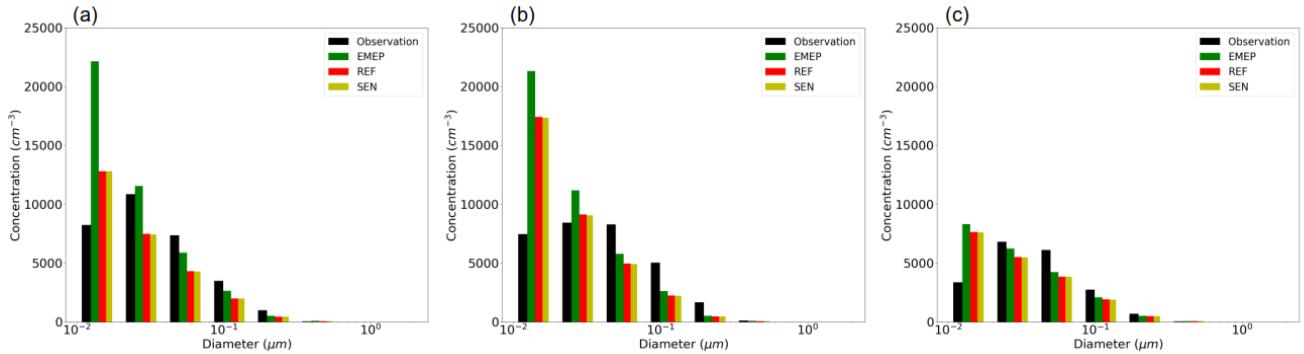
Figure 4. Size distribution of PNC at (a) PA01H, (b) PRG, and (c) SIRTA stations
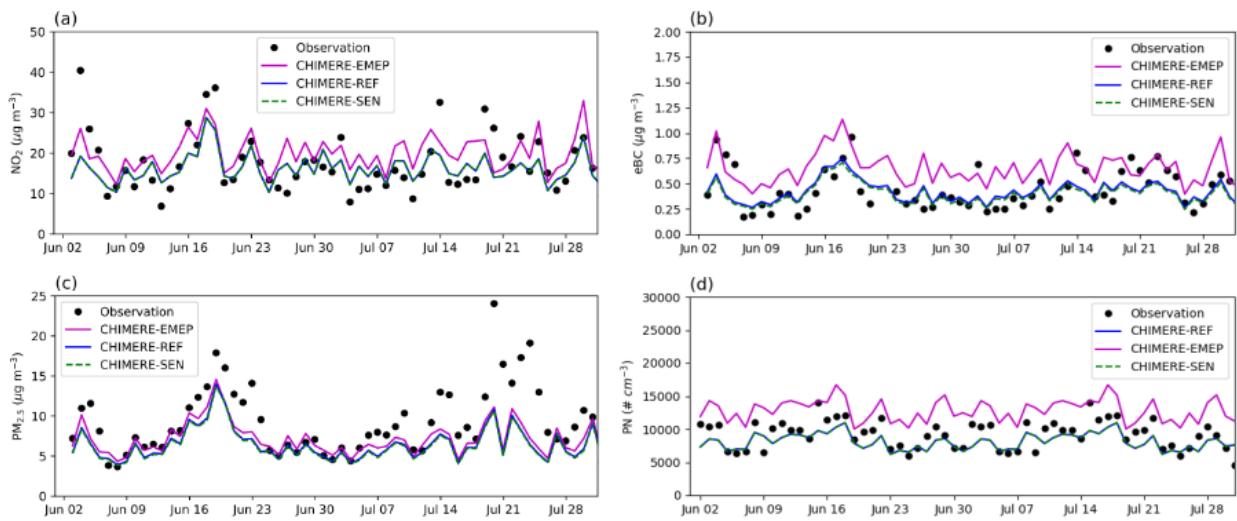
Figure 5. Time series for measured and simulated (a) NO$_2$, (b) eBC, (c) PM$_{2.5}$, and (d) PNC at PA01H station

concentrations simulated by MUNICH are strongly influenced by those of CHIMERE. For example, the peak of concentrations around 19 July is also present at the street scale, but underestimated by the model. In the SEN simulations, eBC and PM$_{2.5}$ concentrations are lower than in the REF simulation due to the reduction of the non-exhaust emissions of small-size sections (0.01 to 2.5 μm). The largest difference are observed at the heavy-traffic station BP_EST (Figure 6 f). Large peaks of eBC concentrations are observed at the BP_EST station. There is greater variability in the measured eBC concentrations compared to those of NO$_2$ at the BP_EST station. This could be due to strong variations in the traffic BC emission factors, or to temporal variations in the EC/BC ratio, which is assumed to be constant.

For PNC, due to the lack of PNC measurement at traffic stations in 2022, for indicative purposes, the concentrations simulated in summer 2022 are compared with the concentrations observed in summer 2021 at two traffic sites (BP_EST and

HAUSS), as documented in the Airparif report (AIRPARIF, 2022). The measurement campaign operated by Airparif took place from 14 June to 19 September 2021 (AIRPARIF, 2022). At PA01H station, the average PNC for particles of diameters between 10 and 400 nm is very close to the average measured in 2022 (about 9,300 # cm^{-3} both in 2021 and 2022). At the two traffic stations (HAUSS and BP_EST), the average PNC measured in the summer 2021 were 17,000 # cm^{-3} and 21,300

345 # cm^{-3} respectively for particles of diameters between 10 and 400 nm. The PNC in the REF (SEN) simulation are 14,500 (14,400) # cm^{-3} at HAUSS and 30,650 (29,800) cm^{-3} at BP_EST, suggesting a bias of 15% at HAUSS and 40% at BP_EST. The wider bias at BP_EST is certainly due to the 10 nm cut-off diameter for the particles. At HAUSS, most of the particle number concentrations is between 10 nm and 400 nm, which represent 94% of particles between 5 and 400 nm. However, at BP_EST, many particles are observed between 5 and 10 nm because of the higher importance of vehicle emissions. The

350 number concentration between 10 and 400 nm represent 86% of the particles between 5 and 400 nm. Although only particles with diameters greater than 10 nm are modelled here, a proportion of particles with smaller diameters is represented, since particles with diameters less than 10 nm are assigned to the first size section (10-20 nm) in the numerical algorithm used here. Although there is a difference in the periods of measurement and simulation with general conditions (traffic emissions, meteorological parameters) that could have been different, the simulated PNC are roughly consistent with the measured ones,

355 and the concentrations in the streets and at the traffic sites are much higher than those in the urban background.

Table 4. Statistical indicators for NO$_2$, eBC, and PM$_{2.5}$ concentrations simulated at the traffic stations in the REF and SEN simulations. The average simulated and observed concentrations are in μg m^{-3} for NO$_2$, eBC, and PM$_{2.5}$. All values respect the strict performance criteria.

	NO$_2$	eBC		PM$_{2.5}$	
	REF/SEN	REF	SEN	REF	SEN
Number of stations	10	3		3	
Observation	40.04	1.26		11.21	
Simulation	38.33	1.26	1.09	9.91	8.56
FB	-0.02	0.09	-0.05	-0.13	-0.27
MG	1.00	0.87	1.00	1.14	1.30
NMSE	0.16	0.20	0.23	0.12	0.17
VG	1.17	1.23	1.21	1.12	1.16
NAD	0.15	0.19	0.19	0.14	0.16
FAC2	0.92	0.89	0.90	0.95	0.95
NMB (%)	1	11	-2	-10	-22
NME (%)	30	40	37	26	29

3.3 Impact of the emission inventory over Greater Paris

The impacts of the emission inventory are investigated over Greater Paris. In the EMEP simulation, the NO$_2$ concentrations are lower by about 15% along the roads and airport than those in the REF simulation, due to higher traffic emissions using the
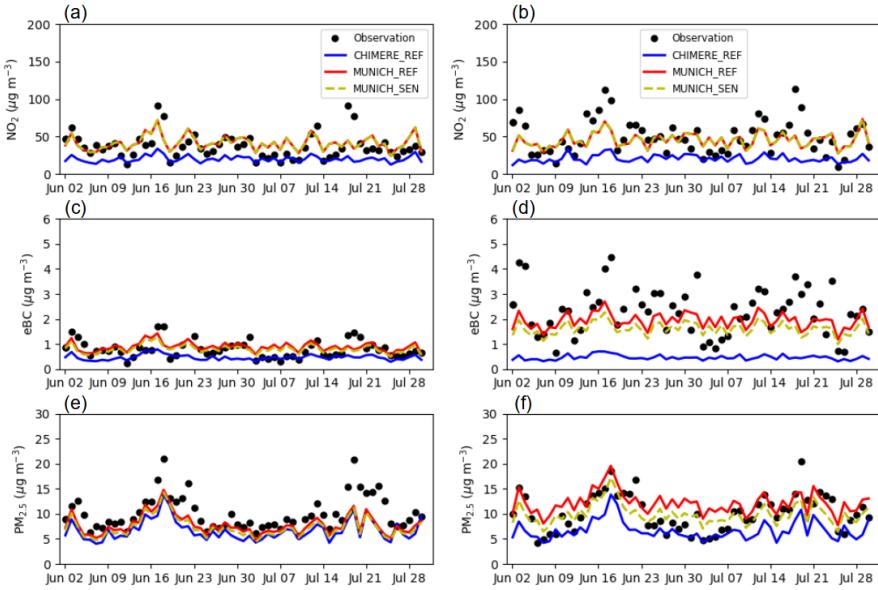
Figure 6. Time series of measured and simulated NO_2 [(a) and (b)], eBC [(c) and (d)], and $PM_{2.5}$ [(e) and (f)] concentrations at the HAUSS (left panels) and BP_EST (right panels) stations.

bottom-up inventory than the EMEP one (Figure C5). In contrast, NO_2 concentrations in areas excluding roads are higher, by
360 about 16%, in the EMEP simulation. The concentrations of NO_2, eBC, $PM_{2.5}$, and PNC in the EMEP simulation are 12%, 50%, 7%, 38% lower, respectively, for Paris compared to those in the REF simulation. The differences in the spatial distributions of eBC and $PM_{2.5}$ concentrations are similar to those of NO_2 concentrations, but the spatial differences are less pronounced than for NO_2. In the eastern region of Greater Paris and the extreme northwest part of the region, PNC are lower using EMEP than the bottom-up inventory owing to lower emissions compared to other areas within the region.

365 Figure 7 shows the average NO_2, eBC, $PM_{2.5}$, and PNC in the REF simulation over Greater Paris with a zoom over Paris down to the street scale. The concentrations are the highest over the center of Paris, and in the main streets of Paris. The spatial gradients of concentrations are stronger for NO_2, eBC, and PNC than for $PM_{2.5}$. $PM_{2.5}$ concentrations are highest over Paris, but high concentrations are also observed at different locations, such as over large woods, due to the formation of secondary organic aerosols. As the lifetime of $PM_{2.5}$ is about a week (Seigneur, 2019), concentrations are relatively homogeneous and
370 high all over Greater Paris. For NO_2, eBC, and PNC, the concentrations are much higher in the main streets than in the urban background than in the suburban and rural areas. The concentrations' spatial gradients may strongly influence the estimation of the population exposure, as detailed in the next section.
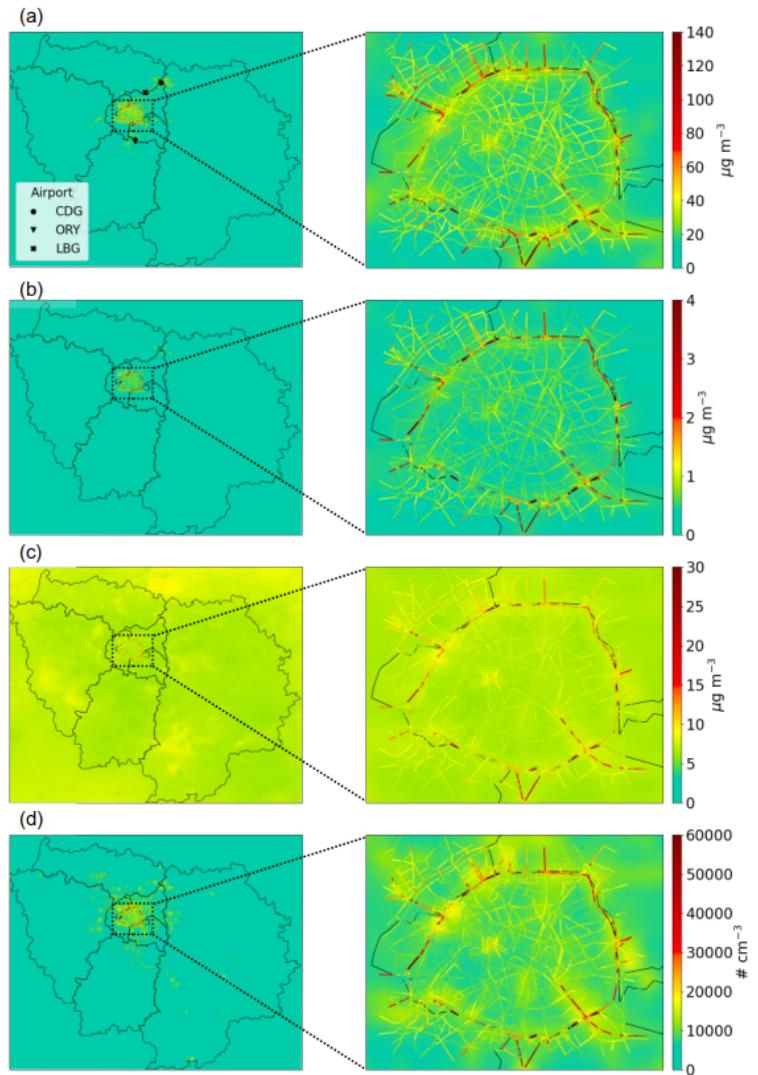
Figure 7. Concentration distribution of the average (a) NO$_2$, (b) eBC, (c) PM$_{2.5}$, and (d) PNC over the period in the REF simulation.

4 Population exposure

As population exposure may be under-estimated using regional-scale modelling, the population-weighted concentration (PWC) and exposure scaling factor (ESF) are calculated for Paris using the multi-scale concentrations and the population data per building. The spatial distributions of PWC for NO$_2$, eBC, PM$_{2.5}$, and PNC are similar to their concentrations (Figure 8), i.e. they have larger values in grid cells with main traffic roads. The average PWC in Paris for NO$_2$, eBC, PM$_{2.5}$, and PNC are 25.3 μg m^{-3}, 0.6 μg m^{-3}, 7.1 μg m^{-3}, and 10963 cm^{-3} in the REF simulation, respectively (Table 5). PWC for eBC, PM$_{2.5}$,
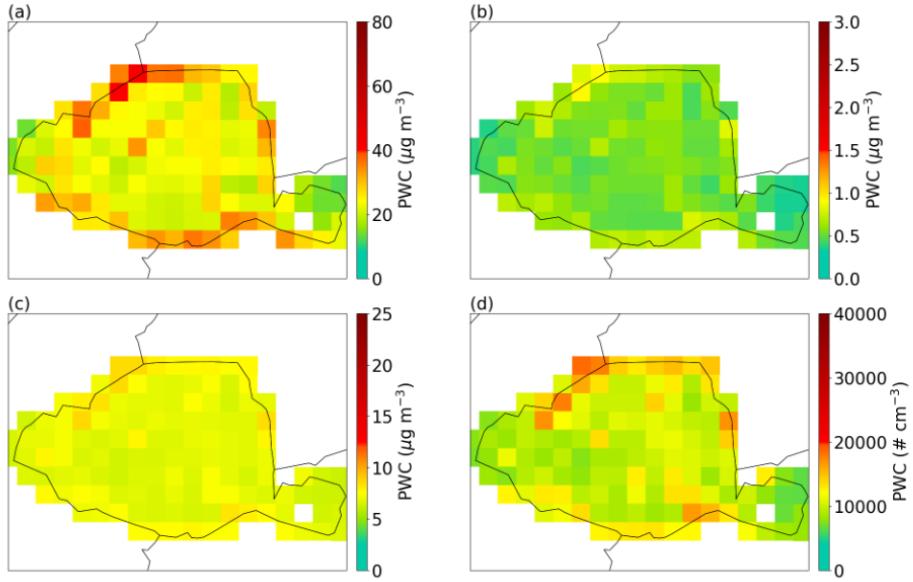
Figure 8. PWC of (a) NO$_2$, (b) eBC, (c) PM$_{2.5}$, and (b) PNC in the REF simulation.

and PNC in the SEN simulation is lower than in the REF simulation. The elevated PWC for NO$_2$, eBC, PM$_{2.5}$, and PNC are
380 observed in heavy-traffic regions in both simulations.

ESF is defined as the ratio of PWC to the regional-scale concentrations simulated by CHIMERE. ESF is higher than 1 for
all pollutants in most areas of Paris (Figure 9). The average ESF over Paris is the highest for NO$_2$, followed by eBC, PNC, and
finally PM$_{2.5}$ (Table 5). For PM$_{2.5}$, the ESF is close to 1 in Paris (1.04 in the REF simulation and 1.02 in the SEN simulation),
because of the low differences between regional and local scale concentrations (Figure 7 c). This suggests that the global
385 Parisian population exposure is reasonably well modelled for PM$_{2.5}$ using regional-scale modelling with 1 km^2 resolution.

For NO$_2$ and eBC, the ESF is about 1.25 in Paris indicating that outdoor population exposure is underestimated by as much
as 25% in Paris urban areas when considering only regional-scale concentrations. For PNC, the ESF is slightly lower (1.12) in
Paris. In heavy-traffic areas, such as in cells that include the very busy Paris ring road, the ESF varies from 1.27 for NO$_2$ and
1.27 for eBC. The ESF is 1.05 for PM$_{2.5}$ along the ring road, indicating that the population exposure is not well represented by
390 regional-scale concentrations for people living next to very busy streets.

5 Conclusion

This study focuses on modelling pollutants of interest to health (NO$_2$, BC, PM$_{2.5}$, and PNC) and with high concentrations
in urban areas, so as to represent the population's exposure to outdoor concentrations as accurately as possible. To do so, a
multi-scale simulation is performed over Greater Paris and down to the street scale over Paris during the summer of 2022 us-
395 ing WRF-CHIMERE/MUNICH/SSH-aerosol. The regional-scale simulation provides a comprehensive representation of urban
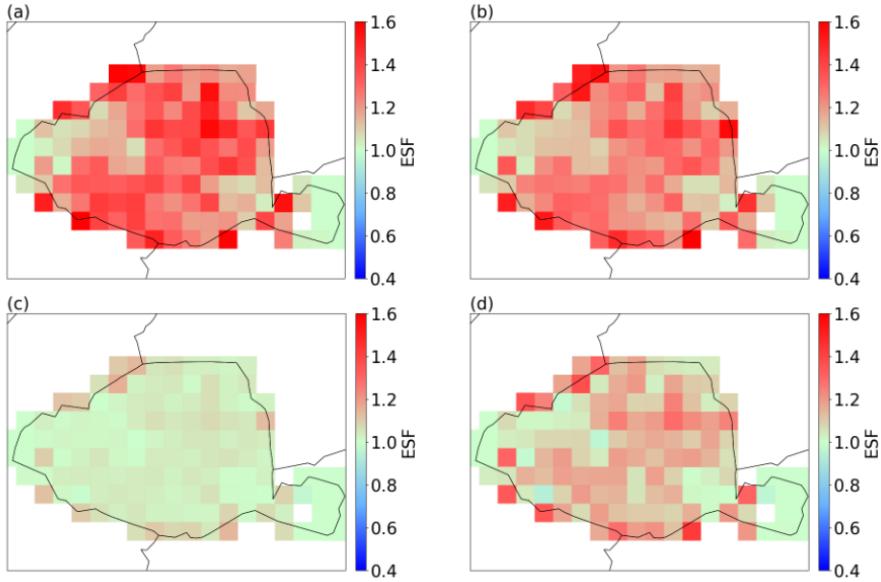
Figure 9. ESF of (a) NO$_2$, (b) eBC, (c) PM$_{2.5}$, and (b) PNC in the REF simulation.

Table 5. Average PWC and ESF for NO$_2$, eBC, PM$_{2.5}$, and PNC over the period of simulation in Paris and Paris Ring Road. PWC is in μg m^{-3} for NO$_2$, BC, PM$_{2.5}$, and in # cm^{-3} for PNC.

		PWC		ESF	
		Paris	Paris Ring road	Paris	Paris Ring Road
REF	NO$_2$	25.34	30.14	1.26	1.27
	eBC	0.57	0.66	1.24	1.27
	PM$_{2.5}$	7.12	7.57	1.04	1.05
	PNC	10963	12816	1.12	1.13
SEN	NO$_2$	25.34	30.14	1.26	1.27
	eBC	0.52	0.59	1.22	1.25
	PM$_{2.5}$	6.81	7.15	1.02	1.03
	PNC	10899	12718	1.12	1.13

background concentrations, but lacks the ability to estimate fine-scale concentrations. Conversely, the street-level simulation adopts a higher spatial resolution and provides more accurate concentration estimates, which are critical for assessing population exposure. The additional computational resources required for street-scale simulation are balanced by the improved accuracy in representing spatial variability, which is essential for effective urban air quality management.

400   In the regional-scale modelling over Greater Paris, the use of two emission inventories was compared: the top-down inventory EMEP and the bottom-up inventory Airparif with correction of the traffic flow using counting loops. The concentrations were

evaluated compared to measurements using strict and less strict criteria from the literature. For regional-scale urban background concentrations, strict criteria are met for NO_2, $PM_{2.5}$, eBC ,and PNC, although the statistics are better for NO_2, eBC, and PNC using the bottom-up inventory than the top-down one. At the street-scale, only the bottom-up inventory is used as it provides traffic emissions per street segments. By comparisons to observations at background and traffic station, the strict criteria are met for NO_2, $PM_{2.5}$, and eBC. As observed, the number of particles is higher on busy streets than in the urban background by a factor of between 1.8 and 3.

The concentrations of NO_2, eBC, $PM_{2.5}$, and PNC in Greater Paris are high in streets, particularly along the Paris Ring Road. Using the top-down inventory, the concentrations tend to be lower in streets than those simulated using the bottom-up inventory, especially for NO_2 concentrations, resulting in less urban heterogeneities. Two estimations of the size distribution of non-exhaust emissions were compared. The impact on eBC and $PM_{2.5}$ is relatively low at the regional scale, by at most a few percents. However, it is higher in heavy-traffic streets, leading to an average impact on the concentrations of eBC, $PM_{2.5}$, and PNC by 9.5%, 6.6%, and 0.7%, respectively.

Population exposure to outdoor concentrations is estimated for Paris by cross-referencing the MAJIC database, which gives the number of inhabitants in each building, with the multi-scale simulations. An exposure scaling factor (ESF) is then calculated to estimate the error made by using the 1 km^2 resolved regional-scale concentrations to approximate outdoor concentrations. The ESF is the highest for eBC, followed by NO_2, PNC, and finally $PM_{2.5}$. The average ESF in Paris is higher than 1 for all pollutants, which indicates that the Parisian population exposure is under-estimated using regional-scale concentrations. Although this under-estimation is low for $PM_{2.5}$, with an ESF of 1.04, it is very high for NO_2 (1.26), eBC (1.24 in REF and 1.22 in SEN), and PNC (1.12). This shows that urban heterogeneities are important to be considered in order to realistically estimate the population exposure to NO_2, eBC, and PNC.

Multi-scale simulations using bottom-up traffic emissions provide innovative and detailed spatially-resolved air-quality information in urban areas. In particular, the ESF may be used to refine the evaluation of population exposure in urban areas employing regional-scale models. The methodologies and findings could be adapted to other major cities, with detailed street-scale emission inventory and street characteristics. This could be done for example, by the continuation of the modelling with the MUNICH model in several cities (Sarica et al., 2023; Wang et al., 2023a; Cevolani et al., 2024). Further investigation is also needed to assess the concentrations and population exposure scaling factors for different seasons.

Code and data availability. The CHIMERE/MUNICH/SSH-aerosol chain used here is available online at https://doi.org/10.5281/zenodo.12639507 (Park et al., 2024).

Hourly NO_2 and $PM_{2.5}$ concentrations measured at the Airparif' stations are available on the Airparif's Open Data Portal: https://data-airparif-asso.opendata.arcgis.com. Regional emissions inventory, as well as hourly BC and PNC data for Paris Châtelet Les Halles, BP-EST and HAUSS stations can be available on request. NO_2 and BC hourly measurements at the HdV station are available on the Aeris data center (https://across.aeris-data.fr/catalogue/). SMPS measurements at SIRTA during the ACROSS campaign can be found on ACROSS data portal https://across.aeris-data.fr. Other measurements at SIRTA are performed within the framework of ACTRIS and can be found on EBAS https://ebas.nilu.no. Level 2 datasets used in the present study from the ACROSS field campaign for the PRG sites are available on the

AERIS datacenter (https://across.aeris-data.fr/catalogue/). The SMPS data obtained at PRG by the SMPS are available using the following DOI 10.25326/658 on the AERIS database. This dataset has the corresponding citation KAMMER, J., SHAHIN, M., D'Anna, B. & Temime-Roussel, B. (2024). ACROSS_LCE_PRG_SMPS_5 min_L2. [dataset]. Aeris. https://doi.org/10.25326/658 The eBC data obtained at PRG by the AE33 are available using the following DOI 10.25326/575 on the AERIS database (https://across.aeris-data.fr/catalogue/) This dataset has the corresponding citation Di Antonio, L., Di Biagio, C. & Gratien, A. (2023). ACROSS_LISA_PRG_AETH-eBC_PM1_1-Min_L2. [dataset]. Aeris. https://doi.org/10.25326/575.

Author contributions. SJP and LL prepared the input data for the CHIMERE/MUNICH model, LL and MV were responsible for the CHIMERE setup and LL performed the CHIMERE simulations. SJP performed the MUNICH simulations. SJP, LL, KS performed the formal analysis. JV, FD and OS provided the regional and traffic emission inventory. OJ determined the formula to discretize the emission size distribution. SJP and YK were responsible for computing the population exposure. SJP and LL conducted the visualization. The experimental data were provided by AB and VG for the Airparif sites; by AG, CDB, LDA, BDA and JK for the PRG site; by JEP for SIRTA; by JEP and OF for the HdV site. KS was responsible for the conceptualization, funding acquisition and supervision. KS, SJP and LL wrote the original draft, and all authors reviewed it.

Competing interests. The authors have no competing interests to declare.

Acknowledgements. This project has also received funding from the European Union's Horizon 2020 research and innovation program under grant agreement No 101036245 (RI-URBANS), and from the French Research project ENZU (Evolution of the Number of Particles in Urban areas) under the program AQACIA/Ademe. BC measurements at the traffic station HdV benefited from the French state aid managed by the ANR under the "Investissements d'avenir" program (ANR-11-IDEX-0004-17-EURE-0006) with support from IPSL/Composair. The measurements at the PRG site have been supported by the ACROSS project. The ACROSS project has received funding from the French National Research Agency (ANR) under the investment program integrated into France 2030 (grant no. ANR-17-MPGA-0002), and it has been supported by the French National program LEFE (Les Enveloppes Fluides et l'Environnement) of the CNRS/INSU (Centre National de la Recherche Scientifique/Institut National des Sciences de L'Univers). The authors also gratefully acknowledge CNRS-INSU for supporting measurements performed at the SI-SIRTA, and those within the long-term monitoring aerosol program SNO-CLAP, both of which are components of the ACTRIS French Research Infrastructure, and whose data is hosted at the AERIS data center (https://www.aeris-data.fr/) This project was provided with computer and storage resources by GENCI at TGCC thanks to the grant A0150114641 on the supercomputer Joliot Curie's the ROME partition. The authors would like to thank Laurent Letinois from INERIS (France) for providing the MAJIC database. The authors would like to thank Alice Maison for discussions on the computation of the Monin-Obukhov length; Matthieu Riva, Rulan Verma and Sebastien Perrier from IRCELYON for nano-SMPS measurements at the PRG site; Shravan Deshmukh and Laurent Poulain for SMPS measurements at the SIRTA site. We thank V. Michoud, C. Cantrell, and J. F. Doussin for the ACROSS project conception and for the coordination of the experimental campaign. Contributions by S. Chevaillier, C. Gaimoz, F. Maisonneuve, M. Cazaunau, and A. Bergé to the experimental deployment at the PRG site are also acknowledged.

Appendix A: Size-discretisation of emissions

A1   Partitioning into two sections by conserving both mass and number

Let M, N be the mass and number concentration of particles contained in a section spanning from diameters d_- to d_+. We
assume that M and N are related by

$$M = N\frac{\pi}{6}\rho\bar{d}^3 \tag{A1}$$

with $\bar{d} = (d_- d_+)^{\frac{1}{2}}$ the geometric mean diameter of the section boundaries.

The section defined by boundaries d_- and d_+ is partitioned in two new sections. For that purpose, we define a new diameter
d_{m} such that $d_- < d_{\mathrm{m}} < d_+$. The first section spans from d_- to d_{m} with mass and number concentrations M_1 and N_1, while
the second section spans from d_{m} to d_+ with mass and number concentrations M_2 and N_2.

Assuming both mass and number conservation, implies

$$M = M_1 + M_2 \tag{A2}$$

$$N = N_1 + N_2 \tag{A3}$$

Furthermore, we enforce a relation similar to (A1) for each section

$$M_1 = N_1 \frac{\pi}{6}\rho(d_- d_{\mathrm{m}})^{\frac{3}{2}} \tag{A4}$$

$$M_2 = N_2 \frac{\pi}{6}\rho(d_{\mathrm{m}} d_+)^{\frac{3}{2}} \tag{A5}$$

Since we have introduced 5 new variables (d_{m}, M_1, M_2, N_1, N_2) and 4 new equations, we should therefore be able to
express mass and number concentrations in the partitions as a function of previous variables and d_{m}.

$$M_1 = N_1 \frac{\pi}{6} \rho (d_- d_{\mathrm{m}})^{\frac{3}{2}} \tag{A6}$$

$$M_1 = (N - N_2) \frac{\pi}{6} \rho (d_- d_{\mathrm{m}})^{\frac{3}{2}} \tag{A7}$$

$$M_1 = M \sqrt{\frac{d_{\mathrm{m}}^3}{d_+^3}} - M_2 \sqrt{\frac{d_-^3}{d_+^3}} \tag{A8}$$

$$M_1 = M \sqrt{\frac{d_{\mathrm{m}}^3}{d_+^3}} - (M - M_1) \sqrt{\frac{d_-^3}{d_+^3}} \tag{A9}$$

Therefore

$$M_1 = M \frac{d_{\mathrm{m}}^{3/2} - d_-^{3/2}}{d_+^{3/2} - d_-^{3/2}} \tag{A10}$$

and similarly

$$M_2 = M \frac{d_+^{3/2} - d_{\mathrm{m}}^{3/2}}{d_+^{3/2} - d_-^{3/2}} \tag{A11}$$

A2 Partitioning into n sections

We wish to upsample our initial section into n sections, defined by the boundaries $\{d_i\}_{i \in (0,n)}$ such that $d_{i-1} < d_i$ for all $i \in (1,n)$. A more general relation for partitioning into n sections can be deduced by noticing that any subsection can be obtained by performing recursively at most two partitions of the whole diameter range.

For the trivial case of the lowest and highest diameter sections, we only need one partitioning operation to deduce their concentrations :

$$M_1 = M \frac{d_1^{3/2} - d_0^{3/2}}{d_n^{3/2} - d_0^{3/2}} \tag{A12}$$

$$M_n = M \frac{d_n^{3/2} - d_{n-1}^{3/2}}{d_n^{3/2} - d_0^{3/2}} \tag{A13}$$

For inner sections such that $1 < i < n$, two successive partitioning operations are necessary. Indeed, by splitting the full diameter range on the lowest diameter of our section of interest and successively splitting the new section on the highest diameter of our section of interest, we have managed to create a section with the boundaries we wished to enforce. The section composition can therefore be inferred.

$$M_i = \left(M \, \frac{d_n^{3/2} - d_{i-1}^{3/2}}{d_n^{3/2} - d_0^{3/2}} \right) \times \frac{d_i^{3/2} - d_{i-1}^{3/2}}{d_n^{3/2} - d_{i-1}^{3/2}} \tag{A14}$$

$$M_i = M \frac{d_i^{3/2} - d_{i-1}^{3/2}}{d_n^{3/2} - d_0^{3/2}} \tag{A15}$$

510   Furthermore, one can easily check that equation (A15) also holds for $i = 1$ and $i = n$.

A3 Partitioning into the 10 sections used here

With the size sections employed in this study and the methodology defined above, the ratios obtained to split emissions in each size section are indicated in Table A1.

Table A1. Ratios employed in PM emissions to split the particle classes into the different size sections

Size section	dmin [μm]	dmax [μm]	PM class	Ratio [%]
1	0.01	0.0199	$PM_{0.1}$	2.91
2	0.0199	0.0398	$PM_{0.1}$	8.27
3	0.0398	0.0794	$PM_{0.1}$	23.24
4	0.0794	0.1585	$PM_{0.1}$	65.58
5	0.1585	0.316	PM_1	26.14
6	0.316	0.631	PM_1	73.86
7	0.631	1.256	$PM_{2.5}$	26.26
8	1.256	2.5	$PM_{2.5}$	73.74
9	2.5	5	PM_{10}	26.12
10	5	10	PM_{10}	73.88

Appendix B: Speciation and calculation of emissions

B1 Non-Traffic Emissions

Anthropogenic emissions are provided for ten different Standard Nomenclature for Air Pollution (SNAP) categories (Tagaris et al., 2015) for NOx, VOC, CO, SO_2, CH_4, $PM_{2.5}$, and PM_{10}. NOx is speciated as 90% NO and 10% NO_2 for all non-traffic categories (Sartelet et al., 2012; Menut et al., 2021; Lugon et al., 2021a). The speciation of coarse and fine PM emissions follows the CAMS set-up (Kuenen et al., 2021), and volatile organic compounds (VOCs) are speciated following Passant (2002). The emissions of condensables, i.e. the sum of intermediate, semi and low volatility organic compounds (IVOC, SVOC, and LVOC, respectively) are estimated by multiplying primary organic matter emitted in each SNAP by 2.5 (Couvidat et al., 2012; Sartelet et al., 2018). Condensable emissions are then divided into volatility classes (32% in IVOC, 43% in SVOC and 25% in LVOC).

The vertical distribution of non-traffic emissions follows Bieser et al. (2011). In the Airparif inventory, a specific analysis was applied to determine the vertical profiles of plane emissions of NOx, PM, CO, SO_2, and VOCs for the three airports (Charles-de-Gaulle (CDG), Paris-Orly (ORY), and Paris–Le Bourget (LBG)) located in Île-de-France (Figure B1). The dataset used for this analysis was obtained from detailed information on flight trajectories for each airport. Specifically, the flight paths were represented as clouds of points in three dimensions (x, y, z), where the altitude (z) was rounded to the nearest 25 meters. The emissions from each airport and pollutant were then summed up to determine the altitudes at which they were produced, and this information was used to create vertical profiles of emissions. These vertical profiles are used to distribute vertically the

530   emissions on the CHIMERE vertical levels. Figure B1 shows the vertical NO_2 and BC emissions profiles at the three airports. Note that the average NO_2 (0.37 μg m^{-2} s^{-1}) and BC (0.04 μg m^{-2} s^{-1}) emissions at the lowest height near the airports are much lower than vehicle emissions of NO_2 (1.65 μg m^{-2} s^{-1}) and BC (0.08 μg m^{-2} s^{-1}) averaged over Greater Paris.
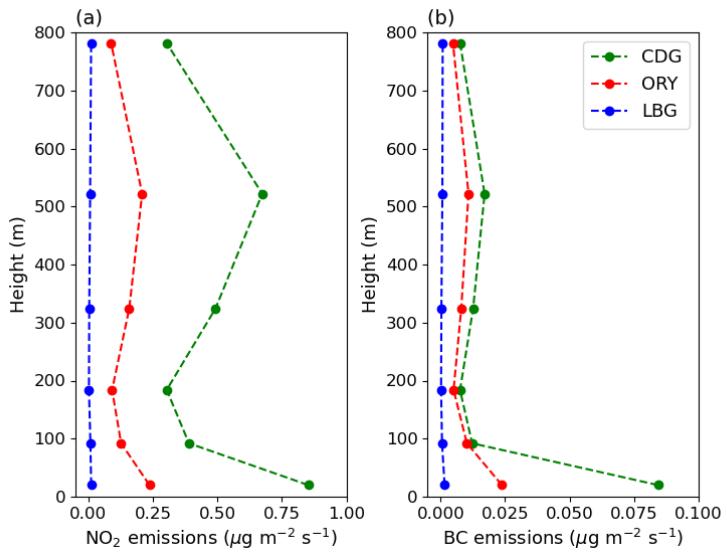
Figure B1. Vertical profiles of the average (a) NO_2 and (b) BC emissions at the airports.

B2   Traffic emissions

The road traffic emissions data were calculated by Airparif using the HEAVEN system, originally developed in 2001 as part
535   of the European project of the same name in partnership with the road traffic management departments of the City of Paris and the Direction Régionale de l'Equipement d'Ile-de-France. Since then, this system has been regularly updated on all its components: emission factors, vehicle fleets, traffic model, real-time counting, network, etc., in order to have the most recent information on vehicle emissions in the Paris region.

     The traffic emissions are calculated hourly for each street and road segment for June and July 2022 over Île-de-France.
540   The traffic emissions inventory was categorized based on emission types (combustion, tire wear, road wear, brake wear, and evaporation), fuel types (electric, gasoline, diesel, Liquefied Petroleum Gas, and Compressed Natural Gas), vehicle types, and Crit'Air classification. In France, the Crit'Air sticker classifies vehicles according to the fine particles and levels of nitrogen oxide that they emit. The vehicle types include passenger vehicles (VP), utility vehicles (VU), heavy vehicles (PL), trailers (TC), and two-wheeled vehicles (2R). The Crit'Air classification depends on the fuel type and the age of the vehicle, as determined
545   from the Euro Norm. The European emission standards (Euro Norm) of the vehicles are estimated from the information on fuel type and Crit'Air classification. Information about the different categories is used to speciate the emissions of the inventory.

The NOx emissions on each road are speciated into NO, NO$_2$, and HONO, depending on the Euro Norm of the vehicles and using speciation from the EMEP guidelines (Leonidas Ntziachristos, 2023b). The average speciation into NO, NO$_2$, and HONO for traffic exhaust emission is 88.5%, 10.6%, and 0.9%, respectively. The traffic emissions of NO$_2$ and BC are illustrated in Figure B2. As expected, emissions are higher during rush hours. Also, NO$_2$ and BC emissions at the BP_EST station, which is next to a heavy-traffic road, are higher than at the HAUSS station (City center). At the city center, NO$_2$ emissions are clearly higher during weekdays than on weekends.

The traffic PM emitted from combustion are assumed to be of diameters lower than 1 μm (PM$_1$) and to be composed of organic matter (OM) and black carbon (BC). The OM/BC ratios differ according to the vehicle fuel, and follow the values proposed in Kostenidou et al. (2021): PM$_{2.5}$ emissions are speciated as 75% of BC and 25% of OM for diesel, while 25% of BC and 75% of OM for gasoline and LPG. The traffic PM emitted from non-exhaust sources are speciated in OM, BC, and inert particles as described in the EMEP/EEA air pollutant emission inventory guidebook. The speciation of Non-Methane VOC follows Theloke and Friedrich (2007), which defines different speciations for gasoline and diesel-powered vehicles. For traffic emissions, the emitted OM is assumed to correspond to LVOC. IVOC and SVOC speciated are speciated based on ratios of Non-methane hydrocarbon emissions, which varies according to the vehicle fuel (Sarica et al., 2023).

The PM emitted from non-exhaust sources (tire, brake, and road wear) are classified as fine (PM$_1$, PM$_{1-2.5}$) and coarse (PM$_{2.5-10}$) particles. They are speciated according to the EMEP guideline (Leonidas Ntziachristos, 2023a), as detailed in Table B1.

Specifically for the simulations using the EMEP emission inventory, as no detailed information is available regarding exhaust and non-exhaust emissions, as well as vehicle categories, the CAMS traffic speciation is employed for PM, and NOx emissions are assumed 90% of NO and 10% of NO$_2$. Also, the total IVOC, SVOC, and LVOC are estimated by multiplying primary organic matter emitted from traffic by 2.5 (Couvidat et al., 2012; Sartelet et al., 2018). For traffic emissions, this total is splitted between 51% of IVOC, 14% of SVOC, and 35% of LVOC.

Table B1. Chemical composition of particles emitted from traffic non-exhaust sources (Leonidas Ntziachristos, 2023a)

	PM$_1$			PM$_{1-2.5}$			PM$_{2.5-10}$		
	Tire	Brake	Road	Tire	Brake	Road	Tire	Brake	Road
BC (%)	30	80	0	21	2	0	0	0	0
OM (%)	70	20	0	48	8	0	0	0	0
Dust (%)	0	0	100	31	90	100	100	100	100

Although street-scale emissions are directly used as input of the street-network model MUNICH, emissions over Greater Paris are gridded, such as being used as input of the CHIMERE model to simulate urban background concentrations.

Appendix C: Supplementary figures
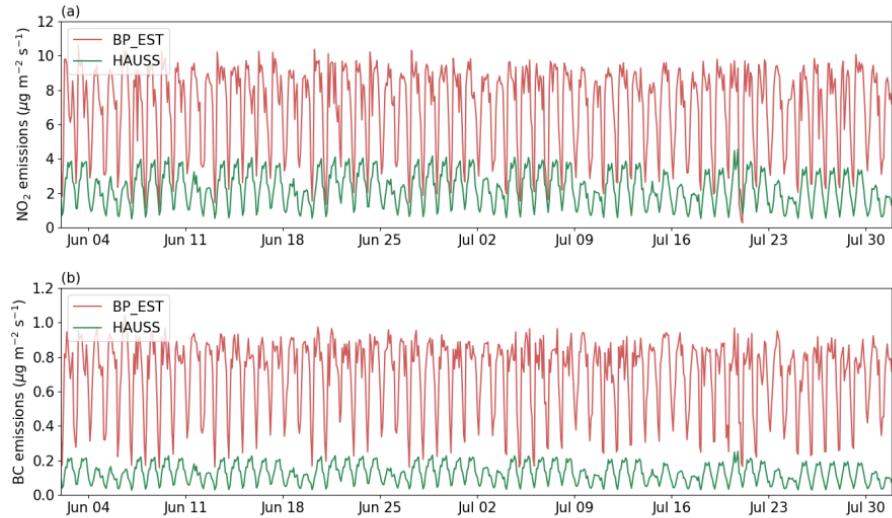
Figure B2. Time series for (a) NO₂ and (b) BC emissions at the HAUSS (city center) and BP_EST (heavy-traffic) stations
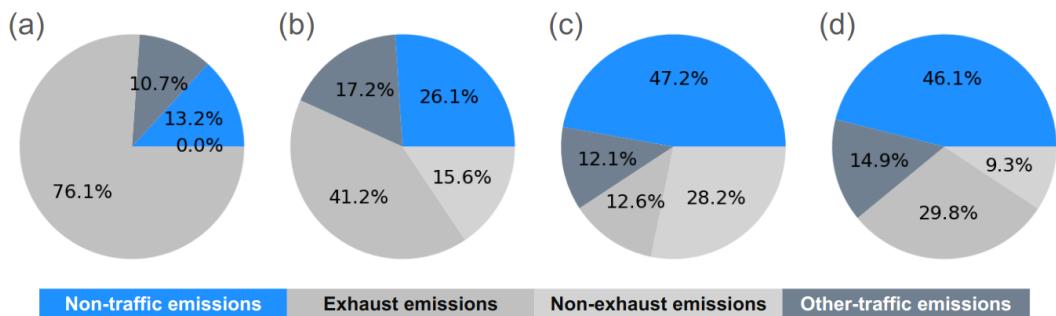
Figure C1. Distribution between vehicular traffic (exhaust and non-exhaust), other traffic and non-traffic emissions for NOx (a), BC (b), PM$_{2.5}$ (c), and PNC (d) in Paris.
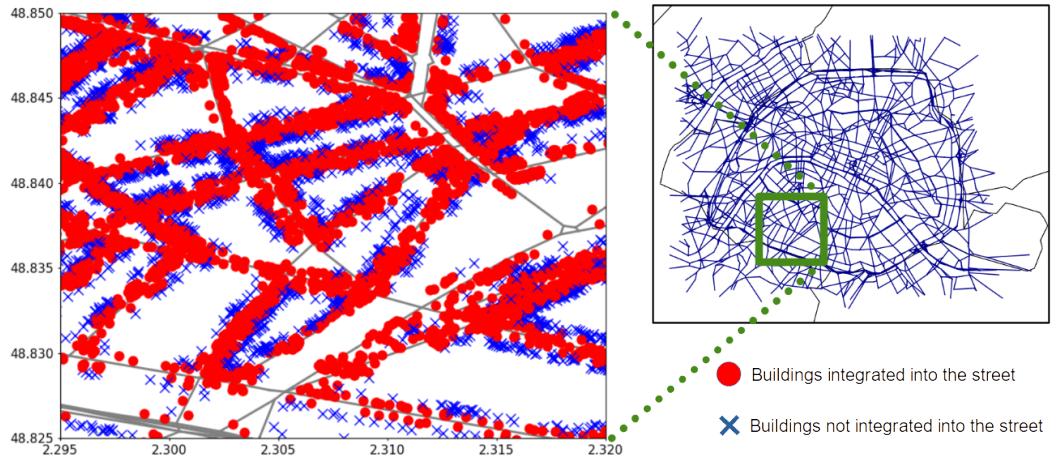
Figure C2. The distribution of buildings according to their integration into the street. The red circles indicate buildings integrated into the street, while the blue crosses indicate buildings that are not integrated into the street.
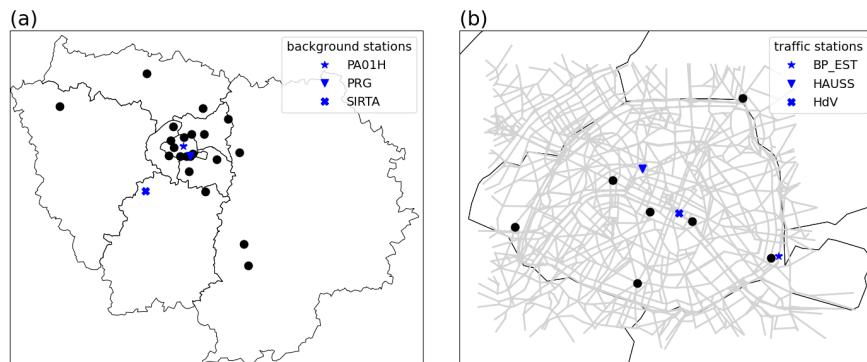
Figure C3. (a) Urban background and (b) traffic stations. Black dots represent the other Airparif stations used in this study.
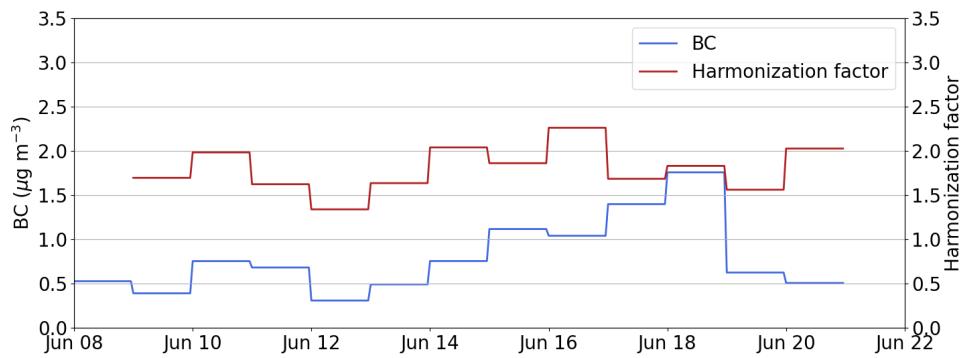
Figure C4. Time series of BC mass and harmonization factor at the PA01H station.
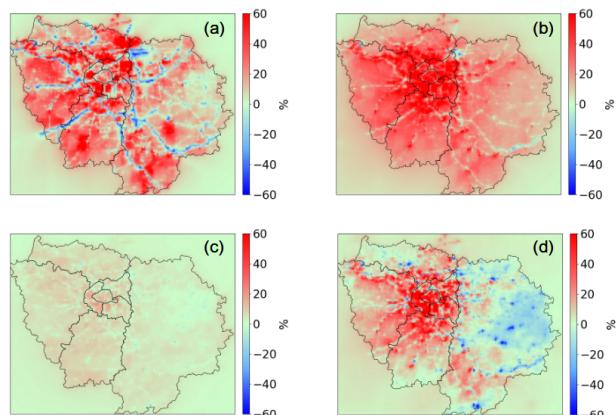
Figure C5. Relative differences (%) in (a) NO$_2$, (b) eBC, (b) PM$_{2.5}$, and (d) PNC between the EMEP and REF simulations.

Appendix D: Statistical parameters

D1   Definitions

$$FB = 2 \cdot (\frac{\overline{O} - \overline{S}}{\overline{O} + \overline{S}})$$

575
$$MG = exp[\overline{ln(O)} - \overline{ln(S)}]$$

$$NMSE = \sqrt{\frac{\overline{(O-S)^2}}{\overline{O \cdot S}}}$$

$$VG = exp[\overline{(ln(O) - \ln(S))^2}]$$

$$NAD = \frac{|\overline{O-S}|}{(\overline{O} + \overline{S})}$$

$$FAC2 = \text{fraction of data that satisfy: } 0.5 \leq \frac{S}{O} \leq 2.0$$

580
$$NMB = \frac{\overline{(S-O)}}{\overline{O}}$$

$$NME = \frac{\overline{|(S-O)|}}{\overline{O}}$$

where O and S represent the observed and simulated concentrations, respectively.

References

Abbou, G., Ghersi, V., Gaie-Levrel, F., Kauffmann, A., Reynaud, M., Debert, C., Quénel, P., and Baudic, A.: Ultrafine Particles
Monitoring in Paris: From Total Number Concentrations to Size Distributions Measurements, Aer. Air. Qual. Res., 24, 240 093,
https://doi.org/10.4209/aaqr.240093, 2024.

Adélaïde, L., Medina, S., Wagner, V., de Crouy-Chanel, P., Real, E., Colette, A., Couvidat, F., Bessagnet, B., Alter, M., Durou, A., Host,
S., Hulin, M., Corso, M., and Pascal, M.: Covid-19 lockdown in spring 2020 in France provided unexpected opportunity to assess health
impacts of falls in air pollution, Front. Sustain. Cities, 3, 643 821, https://doi.org/10.3389/frsc.2021.643821, 2021.

AIRPARIF: Campagne de mesure francilienne sur les particules ultrafines (PUF): Situation de proximité au traffic router été 2021, AIRPARIF
reports, https://www.airparif.fr/sites/default/files/document_publication/Rapport_PUF_Trafic_ete_2021.pdf, 2022.

Andre, M., Sartelet, K., Moukhtar, S., Andre, J., , and Redaelli, M.: Diesel, petrol or electric vehicles: What choices to im-
prove urban air quality in the Ile-de-France region? A simulation platform and case study, Atmos. Environ., 241, 117 752,
https://doi.org/10.1016/j.atmosenv.2020.117752, 2020.

Arino, O., Gross, D., Ranera, F., Leroy, M., Bicheron, P., Brockman, C., Defourny, P., Vancutsem, C., Achard, F., Durieux, L., et al.:
GlobCover: ESA service for global land cover from MERIS, in: 2007 IEEE International Geoscience and Remote Sensing Symposium,
pp. 2412–2415, IEEE, 2007.

Bieser, J., Aulinger, A., Matthias, V., Quante, M., and Van Der Gon, H. D.: Vertical emission profiles for Europe based on plume rise
calculations, Environ. Pollut, 159, 2935–2946, 2011.

Bouma, F., Janssen, N. A., Wesseling, J., van Ratingen, S., Strak, M., Kerckhoffs, J., Gehring, U., Hendricx, W., de Hoogh, K., Ver-
meulen, R., and Hoek, G.: Long-term exposure to ultrafine particles and natural and cause-specific mortality, Environ. Int., 175, 107 960,
https://doi.org/10.1016/j.envint.2023.107960, 2023.

Cantrell, C. and Michoud, V.: An experiment to study atmospheric oxidation chemistry and physics of mixed Anthropogenic–Biogenic air
masses in the Greater Paris area, Bull. Amer. Meteor. Soc., 103, 599–603, https://doi.org/10.1175/BAMS-D-21-0115.1, 2022.

Cevolani, K. T., Lugon, L., Goulart, E. V., and Santos, J. M.: Influence of distinct mobility scenarios on NO2, PM2.5 and PM10 street-level
concentrations. A case study in a Brazilian urban neighborhood, 15, 102 126, https://doi.org/10.1016/j.apr.2024.102126, 2024.

Couvidat, F., Debry, É., Sartelet, K., and Seigneur, C.: A hydrophilic/hydrophobic organic (H^{2}O) aerosol model: Development,
evaluation and sensitivity analysis, J. Geophys. Res. Atmos., 117, 1R, 2012.

Dall'Osto, M., Querol, X., Alastuey, A., O'Dowd, C., Harrison, R. M., Wenger, J., and Gómez-Moreno, F. J.: On the spatial distribution and
evolution of ultrafine particles in Barcelona, Atmos. Chem. Phys., 13, 741–759, https://doi.org/10.5194/acp-13-741-2013, 2013.

Denby, B., Sundvor, I., Johansson, C., Pirjola, L., Ketzel, M., Norman, M., Kupiainen, K., Gustafsson, M., Blomqvist, G., and Omstedt, G.:
A coupled road dust and surface moisture model to predict non-exhaust road traffic induced particle emissions (NORTRIP). Part 1: Road
dust loading and suspension modelling, Atmos. Environ., 77, 283–300, https://doi.org/10.1016/j.atmosenv.2013.04.069, 2013.

Drinovec, L., Močnik, G., Zotter, P., Prévôt, A. S. H., Ruckstuhl, C., Coz, E., Rupakheti, M., Sciare, J., Müller, T., Wiedensohler, A., and
Hansen, A. D. A.: The "dual-spot" Aethalometer: an improved measurement of aerosol black carbon with real-time loading compensation,
Atmos. Meas. Tech., 8, 1965–1979, https://doi.org/10.5194/amt-8-1965-2015, 2015.

Elessa Etuman, A., Coll, I., Viguié, V., Coulombel, N., and Gallez, C.: Exploring urban planning as a lever for emission and exposure control:
Analysis of master plan actions over greater Paris, Atmos. Environ.: X, 22, 100 250, https://doi.org/10.1016/j.aeaoa.2024.100250, 2024.

Fu, X., Xiang, S., Liu, J., Yu, J., Mauzerall, D., and Tao, S.: High-resolution simulation of local traffic-related NOx dispersion and distribution in a complex urban terrain, Environ. Pollut, 263, 114 390, https://doi.org/10.1016/j.envpol.2020.114390, 2020.

Goobie, G., Saha, P., Carlsten, C., Gibson, K., Johannson, K., Kass, D., Ryerson, C., Zhang, Y., Robinson, A., Presto, A., and Nouraie, S.: Ambient ultrafine particulate matter and clinical outcomes in fibrotic interstitial lung disease, Am. J. Respir. Crit. Care Med., 209, 1082–1090, https://doi.org/10.1164/rccm.202307-1275OC, 2024.

Guenther, A., Jiang, X., Heald, C. L., Sakulyanontvittaya, T., Duhl, T., Emmons, L. K., and Wang, X.: The Model of Emissions of Gases and Aerosols from Nature version 2.1 (MEGAN2.1): an extended and upyeard framework for modeling biogenic emissions, Geosci. Model Dev., 5, 1471–1492, https://doi.org/10.5194/gmd-5-1471-2012, 2012.

Guevara, M., Lopez-Aparicio, S., Cuvelier, C., Tarrason, L., Clappier, A., and Thunis, P.: A benchmarking tool to screen and compare bottom-up and top-down atmospheric emission inventories, Air. Qual. Atmos. Health, 10, 627–642, https://doi.org/10.1007/s11869-016-0456-6, 2016.

Haddad, I., Vienneau, D., Daellenbach, K., Modini, R., Slowik, J., Upadhyay, A., Vasilakos, P.N. a Bell, D., Hoogh, K., and Prevot, A.: Opinion: How will advances in aerosol science inform our understanding of the health impacts of outdoor particulate pollution?, Atmos. Chem. Phys., 24, https://doi.org/10.5194/acp-24-11981-2024, 2024.

Haeffelin, M., Barthès, L., Bock, O., Boitel, C., Bony, S., Bouniol, D., Chepfer, H., Chiriaco, M., Cuesta, J., Delanoë, J., Drobinski, P., Dufresne, J.-L., Flamant, C., Grall, M., Hodzic, A., Hourdin, F., Lapouge, F., Lemaître, Y., Mathieu, A., Morille, Y., Naud, C., Noël, V., O'Hirok, W., Pelon, J., Pietras, C., Protat, A., Romand, B., Scialom, G., and Vautard, R.: SIRTA, a ground-based atmospheric observatory for cloud and aerosol research, Annales Geophysicae, 23, 253–275, https://doi.org/10.5194/angeo-23-253-2005, 2005.

Hanna, S. R. and Chang, J. C.: Acceptance criteria for urban dispersion model evaluation, Meteorol. Atmos. Phys., 116, https://doi.org/10.1007/s00703-011-0177-1, 2012.

Herring, S. and Huq, P.: A review of methodology for evaluating the performance of atmospheric transport and dispersion models and suggested protocol for providing more informative results, Fluids, 3, https://doi.org/10.3390/fluids3010020, 2018.

Hoek, G., Vienneau, D., and Hoogh, K.: Does residential address-based exposure assessment for outdoor air pollution lead to bias in epidemiological studies?, Environ. Health, 23:75, https://doi.org/10.1186/s12940-024-01111-0, 2024.

Holnicki, P., Nahorski, Z., and Kaluszko, A.: Impact of vehicle fleet modernization on the traffic-originated air pollution in an urban area—a case study, Atmosphere, 12, 1581, https://doi.org/10.3390/atmos12121581, 2021.

Hood, C., MacKenzie, I., Stocker, J., Johnson, K., Carruthers, D., Vieno, M., and Doherty, R.: Air quality simulations for London using a coupled regional-to-local modelling system, Atmos. Chem. Phys., 18, 11 221–11 245, https://doi.org/10.5194/acp-18-11221-2018, 2018.

Inness, A., Ades, M., Agustí-Panareda, A., Barré, J., Benedictow, A., Blechschmidt, A.-M., Dominguez, J. J., Engelen, R., Eskes, H., Flemming, J., et al.: The CAMS reanalysis of atmospheric composition, Atmos. Chem. Phys., 19, 3515–3556, 2019.

Jereb, B., Gajšek, B., Šipek, G., Kovše, , and Obrecht, M.: Traffic density-related black carbon distribution: Impact of wind in a Basin town, Int. J. Env. Res. Pub. Health, 18, 6490, https://doi.org/10.3390/ijerph18126490, 2021.

Jia, H., Pan, J., Huo, J., Fu, Q., Duan, Y., Lin, Y., Hu, X., and Cheng, J.: Atmospheric black carbon in urban and traffic areas in Shanghai: Temporal variations, source characteristics, and population exposure, Environ. Pollut, 289, 117 868, https://doi.org/10.1016/j.envpol.2021.117868, 2021.

Kamińska, J., Turek, T., Van Popple, M., Peters, J., Hofman, J., and Kazak, J.: Whether cycling around the city is in fact healthy in the light of air quality – Results of black carbon, J. Environ. Manage., 337, https://doi.org/10.1016/j.jenvman.2023.117694, 2023.

Karl, M., Walker, S.-E., Solberg, S., and Ramacher, M. O. P.: The Eulerian urban dispersion model EPISODE – Part 2: Extensions to the source dispersion and photochemistry for EPISODE–CityChem v1.2 and its application to the city of Hamburg, Geosci. Model Dev., 12, 3357–3399, https://doi.org/10.5194/gmd-12-3357-2019, 2019.

Ketzel, M., Frohn, L., Christensen, J. H., Brandt, J., Massling, A., Andersen, C., Im, U., Jensen, S. S., Khan, J., Nielsen, O.-K., Plejdrup, M. S., Manders, A., Denier van der Gon, H., Kumar, P., and Raaschou-Nielsen, O.: Modelling ultrafine particle number concentrations at address resolution in Denmark from 1979 to 2018 - Part 2: Local and street scale modelling and evaluation, Atmos. Environ., 264, 118 633, https://doi.org/10.1016/j.atmosenv.2021.118633, 2021.

Kim, Y., Wu, Y., Seigneur, C., and Roustan, Y.: Multi-scale modeling of urban air pollution: development and application of a Street-in-Grid model (v1.0) by coupling MUNICH (v1.0) and Polair3D (v1.8.1), Geosci. Model Dev., 11, 611–629, https://doi.org/10.5194/gmd-11-611-2018, 2018.

Kim, Y., Lugon1, L., Maison, A., Sarica, T., Roustan, Y., Valari, M., Zhang, Y., André, M., and Sartelet, K.: MUNICH v2.0: a street-network model coupled with SSH-aerosol (v1.2) for multi-pollutant modelling, Geosci. Model Dev., 15, 7371–7396, https://doi.org/10.5194/gmd-15-7371-2022, 2022.

Kostenidou, E., Martinez-Valiente, A., R'Mili, B., Marques, B., Temime-Roussel, B., Durand, A., André, M., Liu, Y., Louis, C., Vansevenant, B., Ferry, D., Laffon, C., Parent, P., and D'Anna, B.: Technical note: Emission factors, chemical composition, and morphology of particles emitted from Euro 5 diesel and gasoline light-duty vehicles during transient cycles, Atmos. Chem. Phys., 21, 4779–4796, https://doi.org/10.5194/acp-21-4779-2021, 2021.

Kuenen, J., Dellaert, S., Visschedijk, A., Jalkanen, J.-P., Super, I., and Denier van der Gon, H.: CAMS-REG-v4: a state-of-the-art high-resolution European emission inventory for air quality modelling, Earth Sys. Sci. Data Discuss., 2021, 1–37, 2021.

Kukkonen, J., Karl, M., Keuken, M. P., Denier van der Gon, H. A. C., Denby, B. R., Singh, V., Douros, J., Manders, A., Samaras, Z., Moussiopoulos, N., Jonkers, S., Aarnio, M., Karppinen, A., Kangas, L., Lützenkirchen, S., Petäjä, T., Vouitsis, I., and Sokhi, R. S.: Modelling the dispersion of particle numbers in five European cities, Geosci. Model Dev., 9, 451–478, https://doi.org/10.5194/gmd-9-451-2016, 2016.

Kuklinska, K., Wolska, L., and Namiesnik, J.: Air quality policy in the U.S. and the EU and – a review, 2015.

Kulmala, M., Asmi, A., Lappalainen, H., Baltensperger, U., Brenguier, J.-L., Facchini, M., Hansson, H.-C., Hov, o., O'Dowd, C., Pöschl, U., Wiedensohler, A., Boers, R., Boucher, O., de Leeuw, G., Denier van der Gon, H., Feichter, J., Krejci, R., Laj, P., Lihavainen, H., Lohmann, U., McFiggans, G., Mentel, T., Pilinis, C., Riipinen, I., Schulz, M., Stohl, A., Swietlicki, E., Vignati, E., Alves, C., Amann, M., Ammann, M., Arabas, S., Artaxo, P., Baars, H., Beddows, D., Bergström, R., Beukes, J., Bilde, M., Burkhart, J., Canonaco, F., Clegg, S., Coe, H., Crumeyrolle, S., D'Anna, B., Decesari, S., Gilardoni, S., Fischer, M., Fjaeraa, A., Fountoukis, C., George, C., Gomes, L., Halloran, P., Hamburger, T., Harrison, R., Herrmann, H., Hoffmann, T., Hoose, C., Hu, M., Hyvärinen, A., Hõrrak, U., Iinuma, Y., Iversen, T., Josipovic, M., Kanakidou, M., Kiendler-Scharr, A., Kirkevåg, A., Kiss, G., Klimont, Z., Kolmonen, P., Komppula, M., Kristjánsson, J.-E., Laakso, L., Laaksonen, A., Labonnote, L., Lanz, V., Lehtinen, K., Rizzo, L., Makkonen, R., Manninen, H., McMeeking, G., Merikanto, J., Minikin, A., Mirme, S., Morgan, W., Nemitz, E., O'Donnell, D., Panwar, T. S., Pawlowska, H., Petzold, A., Pienaar, J., Pio, C., Plass-Duelmer, C., Prévôt, A., Pryor, S., Reddington, C., Roberts, G., Rosenfeld, D., Schwarz, J., Seland, o., Sellegri, K., Shen, X., Shiraiwa, M., Siebert, H., Sierau, B., Simpson, D., Sun, J., Topping, D., Tunved, P., Vaattovaara, P., Vakkari, V., Veefkind, J., Visschedijk, A., Vuollekoski, H., Vuolo, R., Wehner, B., Wildt, J., Woodward, S., Worsnop, D., van Zadelhoff, G.-J., Zardini, A., Zhang, K., van Zyl, P., Kerminen, V.-M., Carslaw, K., and Pandis, S.: General overview: European Integrated project on Aerosol Cloud Climate and Air Quality interactions (EUCAARI) –

integrating aerosol research from nano to global scales, Atmos. Chem. Phys., 11, 13 061–13 143, https://doi.org/10.5194/acp-11-13061-2011, 2011.

695 Kusaka, H., Kondo, H., Kikegawa, Y., and Kimura, F.: A simple single-layer urban canopy model for atmospheric models: Comparison with multi-layer and slab models, Bound-Lay Meteorol., 101, 329–358, 2001.

Kwak, K.-H., Baik, J.-J., Ryu, Y.-H., and Lee, S.-H.: Urban air quality simulation in a high-rise building area using a CFD model coupled with mesoscale meteorological and chemistry-transport models, Atmos. Environ., 100, 167–177, https://doi.org/10.1016/j.atmosenv.2014.10.059, 2015.

700 Kwon, H., Ryu, M., and Carlsten, C.: Ultrafine particles: unique physicochemical properties relevant to health and disease, Exp Mol Med., 52, 318–328, https://doi.org/10.1038/s12276-020-0405-1, 2020.

Lee, S.-H. and Kwak, K.-H.: Assessing 3-D spatial extent of near-road air pollution around a signalized intersection using drone monitoring and WRF-CFD modeling, Int. J. Env. Res. Pub. Health, 17, 6915, https://doi.org/10.3390/ijerph17186915, 2020.

Leonidas Ntziachristos, P. B.: 1.A.3.b.vi Road transport: Automobile tyre and brake wear 1.A.3.b.vii Road transport: Automobile road
705 abrasion. In: European Environment Agency (EEA): EMEP/EEA air pollutant emission inventory guidebook, 2023a.

Leonidas Ntziachristos, Z. S.: 1.A.3.b.i, 1.A.3.b.ii, 1.A.3.b.iii, 1.A.3.b.ivPassenger cars, light commercial trucks, heavy-duty vehicles including buses and motor cycles. In: European Environment Agency (EEA): EMEP/EEA air pollutant emission inventory guidebook, 2023b.

Lequy, E., Siemiatycki, J., Hoogh, K., Vienneau, D., Dupuy, J., Garès, V., Hertel, O., Christensen, J., Zhivin, S., Goldberg, M., Zins, M., , and Jacquemin, B.: Contribution of long-term exposure to outdoor black carbon to the carcinogenicity of air pollution: Evidence regarding
710 risk of cancer in the Gazel Cohort, Environ. Health Perspect., 2021.

Lequy, E., Zare Sakhvidi, M. J., Vienneau, D., de Hoogh, K., Chen, J., Dupuy, J.-F., Garès, V., Burte, E., Bouaziz, O., Le Tertre, A., Wagner, V., Hertel, O., Christensen, J. H., Zhivin, S., Siemiatycki, J., Goldberg, M., Zins, M., and Jacquemin, B.: Influence of exposure assessment methods on associations between long-term exposure to outdoor fine particulate matter and risk of cancer in the French cohort Gazel, Sci. Total Environ., 820, 153 098, https://doi.org/10.1016/j.scitotenv.2022.153098, 2022.

715 Li, F., Luo, B., Zhai, M., Liu, L., Zhao, G., Xu, H., Deng, T., Deng, X., Tan, H., Kuang, Y., and Zhao, J.: Black carbon content of traffic emissions significantly impacts black carbon mass size distributions and mixing states, Atmos. Chem. Phys., 23, 6545–6558, https://doi.org/10.5194/acp-23-6545-2023, 2023a.

Li, G., Lu, P., Deng, S., Gao, J., Lu, Z., and Li, Q.: Spatial variability and health assessment of particle number concentration at different exposure locations near urban traffic arterial: A case study in Xi'an, China, Atmos. Environ., 314,
720 https://doi.org/10.1016/j.atmosenv.2023.120086, 2023b.

Lin, C., Wang, Y., Ooka, R., Flageul, C., Kim, Y., Kikumoto, H., Wang, Z., and Sartelet, K.: Modeling of street-scale pollutant dispersion by coupled simulation of chemical reaction, aerosol dynamics, and CFD, Atmos. Chem. Phys., 23, 1421–1436, https://doi.org/10.5194/acp-23-1421-2023, 2023.

Lopez-Aparicio, S., Guevara, M., Thunis, P., and Cuvelier, K.: Assessment of discrepancies between bottom-up and regional emission
725 inventories in Norwegian urban areas, Atmos. Environ., 154, 285–296, https://doi.org/10.1016/j.atmosenv.2017.02.004, 2017.

Lugon, L., Sartelet, K., Kim, Y., Vigneron, J., and Chrétien, O.: Simulation of primary and secondary particles in the streets of Paris using MUNICH, Faraday Discuss., 226, 432–456, https://doi.org/10.1039/D0FD00092B, 2021a.

Lugon, L., Vigneron, J., Debert, C., Chrétien, O., and Sartelet, K.: Black carbon modeling in urban areas: investigating the influence of resuspension and non-exhaust emissions in streets using the Street-in-Grid model for inert particles (SinG-inert), Geosci. Model Dev., 14,
730 7001–7019, https://doi.org/10.5194/gmd-14-7001-2021, 2021b.

Lugon, L., Kim, Y., Vigneron, J., Chrétien, O., André, M., André, J., Moukhtar, S., Redaelli, M., and Sartelet, K.: Effect of vehicle fleet composition and mobility on outdoor population exposure: A street resolution analysis in Paris, Atmos. Pollut. Res., 13, 101 365, https://doi.org/10.1016/j.apr.2022.101365, 2022.

Létinois, L.: Methodologie de repartition spatiale de la population - http://www.lcsqa.org/rapport/2014/ineris/methodologie-repartition-spatiale-population, Rapport LCSQA, http://www.lcsqa.org/rapport/2014/ineris/methodologie-repartition-spatiale-population, 2014.

Ma, X., Zou, B., Deng, J., Gao, J., Longley, I., Xiao, S., Guo, B., Wu, Y., Xu, T., Xu, X., Yang, X., Wang, X., Tan, Z., Wang, Y., Morawska, L., and Salmond, J.: A comprehensive review of the development of land use regression approaches for modeling spatiotemporal variations of ambient air pollution: A perspective from 2011 to 2023, Environ. Int., 183, 108 430, https://doi.org/10.1016/j.envint.2024.108430, 2024.

Maison, A., Lugon, L., Park, S.-J., Baudic, A., Cantrell, C., Couvidat, F., D'Anna, B., Di Biagio, C., Gratien, A., Gros, V., Kalalian, C., Kammer, J., Michoud, V., Petit, J.-E., Shahin, M., Simon, L., Valari, M., Vigneron, J., Tuzet, A., and Sartelet, K.: Significant impact of urban-tree biogenic emissions on air quality estimated by a bottom-up inventory and chemistry-transport modeling, Atmos. Chem. Phys., 24, 6011–6046, https://doi.org/10.5194/acp-24-6011-2024, 2024a.

Maison, A., Lugon, L., Park, S.-J., Boissard, C., Faucheux, A., Gros, V., Kalalian, C., Kim, Y., Leymarie, J., Petit, J.-E., Roustan, Y., Sanchez, O., Squarcioni, A., Valari, M., Viatte, C., Vigneron, J., Tuzet, A., and Sartelet, K.: Contrasting effects of urban trees on air quality: From the aerodynamic effects in streets to impacts of biogenic emissions in cities, Sci. Total Environ., 946, 174 116, https://doi.org/10.1016/j.scitotenv.2024.174116, 2024b.

Mao, X., Guo, X., Chang, Y., and Peng, Y.: Improving air quality in large cities by substituting natural gas for coal in China: changing idea and incentive policy implications, Energy Policy, 33, 307–318, https://doi.org/10.1016/j.enpol.2003.08.002, 2005.

Menut, L., Bessagnet, B., Briant, R., Cholakian, A., Couvidat, F., Mailler, S., Pennel, R., Siour, G., Tuccella, P., Turquety, S., and Valari, M.: The CHIMERE v2020r1 online chemistry-transport model, Geosci. Model Dev., 14, 6781–6811, https://doi.org/10.5194/gmd-14-6781-2021, 2021.

Menut, L., Cholakian, A., Siour, G., Lapere, R., Pennel, R., Mailler, S., and Bessagnet, B.: Impact of Landes forest fires on air quality in France during the 2022 summer, Atmos. Chem. Phys., 23, 7281–7296, https://doi.org/10.5194/acp-23-7281-2023, 2023.

Musson-Genon, L., G. S. B. E.: A simple method to determine evaporation, duct height in the sea surface boundary layer, Radio Science, 27, 635–644, 1992.

Ntziachristos, L., B. P.: 1. A. 3. b. vi road transport: automobile tyre and brake wear; 1. a. 3. b. vii road tranport: automobile road abration. In: European Environment Agency (EEA): EMEP/EEA air pollutant emission inventory guidebook, 2016.

Olin, M., Patoulias, D., Kuuluvainen, H., Niemi, J., Rönkkö, T., Pandis, S., Riipinen, I., and Dal Maso, M.: Contribution of traffic-originated nanoparticle emissions to regional and local aerosol levels, Atmos. Chem. Phys., 22, 1131–1148, https://doi.org/10.5194/acp-22-1131-2022, 2022.

Ostro, B., Hu, J., Goldberg, D., Reynolds, P., Hertz, A., Bernstein, L., and Kleeman, M.: Associations of mortality with long-term exposures to fine and ultrafine particles, species and sources: results from the California Teachers Study Cohort, Environ Health Perspect., 123, 549–556, https://doi.org/10.1289/ehp.1408565, 2015.

Park, M., Joo, H., Lee, K., Jang, M., Kim, S., Kim, I., Borlaza, L., Lim, H., Shin, H., Chung, K., Choi, Y.-H., Park, S., Bae, M.-S., Lee, J., Song, H., and Park, K.: Differential toxicities of fine particulate matters from various sources, Sci. Rep., 8, 17 007, https://doi.org/10.1038/s41598-018-35398-0, 2018.

Park, S.-J., Kang, G., Choi, W., Kim, D.-Y., Kim, J.-S., and J.-J., K.: Effects of fences and green zones on the air flow and $PM_{2.5}$ concentration around a school in a building-congested district, Applied Sciences, 11, 9216, https://doi.org/10.3390/app11199216, 2021.

Passant, N.: Speciation of UK emissions of non-methane volatile organic compounds, AEA Technology, 2002.

770 Patoulias, D. and Pandis, S.: Simulation of the effects of low volatility organic compounds on aerosol number concentrations in Europe, Atmos. Chem. Phys., 22, 1689–1706, https://doi.org/10.5194/acp-22-1689-2022, 2022a.

Patoulias, D. and Pandis, S. N.: Simulation of the effects of low-volatility organic compounds on aerosol number concentrations in Europe, Atmos. Chem. Phys., 22, 1689–1706, https://doi.org/10.5194/acp-22-1689-2022, 2022b.

Piscitello, A., Bianco, C., Casasso, A., and Sethi, R.: Non-exhaust traffic emissions: Sources, characterization, and mitigation measures, Sci.
775 Total Environ., 766, 144 440, https://doi.org/10.1016/j.scitotenv.2020.144440, 2021.

Powers, J. G., Klemp, J. B., Skamarock, W. C., Davis, C. A., Dudhia, J., Gill, D. O., Coen, J. L., Gochis, D. J., Ahmadov, R., Peckham, S. E., et al.: The Weather Research and Forecasting model: Overview, system efforts, and future directions, Bull. Amer. Meteor. Soc., 98, 1717–1737, 2017.

Sarica, T., Sartelet, K., Roustan, Y., Kim, Y., Lugon, L., Marques, B., D'Anna, B., Chaillou, C., and Larrieu, C.: Sen-
780 sitivity of pollutant concentrations in urban streets to asphalt and traffic-related emissions, Environ. Pollut, 332, 121 955, https://doi.org/10.1016/j.envpol.2023.121955, 2023.

Sartelet, K., Couvidat, F., Seigneur, C., and Roustan, Y.: Impact of biogenic emissions on air quality over Europe and North America, Atmos. Environ., 53, 131–141, https://doi.org/10.1016/j.atmosenv.2011.10.046, 2012.

Sartelet, K., Zhu, S., Moukhtar, S., André, M., André, J., Gros, V., Favez, O., Brasseur, A., and Redaelli, M.: Emission of intermediate, semi
785 and low volatile organic compounds from traffic and their impact on secondary organic aerosol concentrations over Greater Paris, Atmos. Environ., 180, 126–137, 2018.

Sartelet, K., Couvidat, F., Wang, Z., Flageul, C., and Kim, Y.: SSH-Aerosol v1.1: A modular box model to simulate the evolution of primary and secondary aerosols, Atmosphere, 11, 525, https://doi.org/10.3390/atmos11050525, 2020.

Sartelet, K., Kim, Y., Couvidat, F., Merkel, M., Petäjä, T., Sciare, T., and Wiedensohler, A.: Influence of emission size distribution and
790 nucleation on number concentrations over Greater Paris, Atmos. Chem. Phys., 22, 8579–8596, https://doi.org/10.5194/acp-22-8579-2022, 2022.

Sartelet, K., Wang, Z., Lannuque, V., Iyer, S., Couvidat, F., and Sarica, T.: Modelling molecular composition of SOA from toluene photo-oxidation at urban and street scales, Environ. Sci.: Atmos., 4, 839–847, https://doi.org/10.1039/D4EA00049H, 2024.

Savadkoohi, M., Pandolfi, M., Reche, C., Niemi, J., Mooibroek, D., Titos, G., Green, D., Tremper, A., Hueglin, C., Liakakou, E., Mi-
795 halopoulos, N., Stavroulas, I., Artiñano, B., Coz, E., Alados-Arboledas, L., Beddows, D., Riffault, V., Brito, J., Bastian, S., Baudic, A., Colombi, C., Costabile, F., Chazeau, B., Marchand, N., Gómez-Amo, J., Estellés, V., Matos, V., Gaag, E., Gille, G., Luoma, K., Manninen, H., Norman, M., Silvergren, S., Petit, J., Putaud, J., Rattigan, O., Timonen, H., Tuch, T., Merkel, M., Weinhold, K., Vratolis, S., Vasilescu, J., Favez, O., Harrison, R., Laj, P., Wiedensohler, A., Hopke, P., Petäjä, T., Alastuey, A., and Querol, X.: The variability of mass concentrations and source apportionment analysis of equivalent black carbon across urban Europe, Environ. Int., 178, 108 081,
800 https://doi.org/10.1016/j.envint.2023.108081, 2023.

Savadkoohi, M., Pandolfi, M., Favez, O., Putaud, J.-P., Eleftheriadis, K., Fiebig, M., Hopke, P., Laj, P., Wiedensohler, A., Alados-Arboledas, L., Bastian, S., Chazeau, B., María, , Colombi, C., Costabile, F., Green, D., Hueglin, C., Liakakou, E., Luoma, K., Listrani, S., Mihalopoulos, E., Marchand, E., Močnik, G., Niemi, J., Ondráček, J., Petit, J.-E., Rattigan, O., Reche, C., Timonen, H., Titos, G., Tremper, A., Vratolis, S., Vodička, P., Funes, E., Zíková, N., Harrison, R., Petäjä, T., Alastuey, A., and Querol, X.: Recommendations for reporting
805 equivalent black carbon (eBC) mass concentrations based on long-term pan-European in-situ observations, Environ. Int., 185, 108 553, https://doi.org/10.1016/j.envint.2024.108553, 2024.

Schwarz, M., Schneider, A., Cyrys, J., Bastian, S., Breitner, S., and Peters, A.: Impact of Ambient Ultrafine Particles on Cause-Specific Mortality in Three German Cities, American Journal of Respiratory and Critical Care Medicine, 207, 1334–1344, https://doi.org/10.1164/rccm.202209-1837OC, 2023.

810 Seigneur, C.: Air pollution: Concepts, theory, and applications, Cambridge University Press, 2019.

Selmi, W., Weber, C., Rivière, E., Blond, N., Mehdi, L., and Nowak, D.: Air pollution removal by trees in public green spaces in Strasbourg city, France, Urban For. Urban Green, 17, 192–201, https://doi.org/10.1016/j.ufug.2016.04.010, 2016.

Soulhac, L., Salizzoni, P., Cierco, F., and Perkins, R.: The model SIRANE for atmospheric urban pollutant dispersion; part I, presentation of the model, Atmos. Environ., 45, 7379–7395, https://doi.org/10.1016/j.atmosenv.2011.07.008, 2011.

815 Southerland, V., Brauer, M., Mohegh, A., Hammer, M., van Donkelaar, A., Martin, R., Apte, J., and Anenberg, S.: Global urban temporal trends in fine particulate matter (PM_{25}) and attributable health burdens: estimates from global datasets, Lancet Planet Health, 6, 139–146, https://doi.org/10.1016/S2542-5196(21)00350-8, 2022.

Squarcioni, A., Roustan, Y., Valari, M., Kim, Y., Sartelet, K., Lugon, L., Dugay, F., and Voitot, R.: To what extent is the description of streets important in estimating local air-quality? A case study over Paris, EGUsphere, 2024, 1–43, https://doi.org/10.5194/egusphere-2024-1043, 820 2024.

Strömberg, J., Li, X., Kurppa, M., Kuuluvainen, H., Pirjola, L., and Järvi, L.: Effect of radiation interaction and aerosol processes on ventilation and aerosol concentrations in a real urban neighbourhood in Helsinki, Atmos. Chem. Phys., 23, 9347–9364, https://doi.org/10.5194/acp-23-9347-2023, 2023.

Tagaris, E., Sotiropoulou, R., Gounaris, N., Andronopoulos, S., and Vlachogiannis, D.: Effect of the Standard Nomenclature for Air Pollution 825 (SNAP) categories on air quality over Europe, Atmosphere, 6, 1119–1128, https://doi.org/10.3390/atmos6081119, 2015.

Theloke, J. and Friedrich, R.: Compilation of a database on the composition of anthropogenic VOC emissions for atmospheric modeling in Europe, Atmos. Environ., 41, 4148–4160, 2007.

Tomar, G., Nagpure, A., Kumar, V., and Jain, Y.: High resolution vehicular exhaust and non-exhaust emission analysis of urban-rural district of India, Sci. Total Environ., 805, 150 255, https://doi.org/10.1016/j.scitotenv.2021.150255, 2022.

830 Trechera, P., Garcia-Marlès, M., Liu, X., Reche, C., Pérez, N., Savadkoohi, M., Beddows, D., Salma, I., Vorosmarty, M., Casans, A., Casquero-Vera, J. A., Hueglin, C., Marchand, N., Chazeau, B., Gille, G., Kalkavouras, P., Mihalopoulos, N., Ondracek, J., Zikova, N., Niemi, J. V., Manninen, H. E., Green, D. C., Tremper, A. H., Norman, M., Vratolis, S., Eleftheriadis, K., Gomez-Moreno, F. J., Alonso-Blanco, E., Gerwig, H., Wiedensohler, A., Weinhold, K., Merkel, M., Bastian, S., Petit, J.-E., Favez, O., Crumeyrolle, S., Ferlay, N., Martins Dos Santos, S., Putaud, J.-P., Timonen, H., Lampilahti, J., Asbach, C., Wolf, C., Kaminski, H., Altug, H., Hoffmann, B., Rich, 835 D. Q., Pandolfi, M., Harrison, R. M., Hopke, P. K., Petäjä, T., Alastuey, A., and Querol, X.: Phenomenology of ultrafine particle concentrations and size distribution across urban Europe, Environ. Int., 172, 107 744, https://doi.org/10.1016/j.envint.2023.107744, 2023.

Valari, M. and Menut, L.: Transferring the heterogeneity of surface emissions to variability in pollutant concentrations over urban areas through a chemistry-transport model, Atmos. Environ., 44, 3229–3238, https://doi.org/10.1016/j.atmosenv.2010.06.001, 2010.

Valari, M., Markakis, K., Powaga, E., Collignan, B., and Perrussel, O.: EXPLUME v1.0: a model for personal exposure to ambient O_3 and 840 $PM_{2.5}$, Geosci. Model Dev., 13, 1075–1094, https://doi.org/10.5194/gmd-13-1075-2020, 2020.

Wang, T., Liu, H., Li, J., Wang, S., Kim, Y., Sun, Y., Yang, W., Du, H., Wang, Z., and Wang, Z.: A two-way coupled regional urban–street network air quality model system for Beijing, China, Geosci. Model Dev., 16, 5585–5599, https://doi.org/10.5194/gmd-16-5585-2023, 2023a.

Wang, Y., Ma, Y., Muñoz-Esparza, D., Dai, J., Li, C., Lichtig, P., Tsang, R., Liu, C., Wang, T., and Brasseur, G.: Coupled mesoscale–microscale modeling of air quality in a polluted city using WRF-LES-Chem, Atmos. Chem. Phys., 23, 5905–5927, https://doi.org/10.5194/acp-23-5905-2023, 2023b.

WHO: WHO global air quality guidelines: particulate matter ($PM_{2.5}$ and PM_{10}), ozone, nitrogen dioxide, sulfur dioxide and carbon monoxide., WHO reports, https://iris.who.int/bitstream/handle/10665/345329/9789240034228-eng.pdf, 2021.

Yuan, C., Ng, E., and Norford, L.: Improving air quality in high-density cities by understanding the relationship between air pollutant dispersion and urban morphologies, Build. Environ., 71, 245–258, https://doi.org/10.1016/j.buildenv.2013.10.008, 2014.

Zhong, J., Harrison, R. M., James Bloss, W., Visschedijk, A., and Denier van der Gon, H.: Modelling the dispersion of particle number concentrations in the West Midlands, UK using the ADMS-Urban model, Environ. Int., 181, 108 273, https://doi.org/10.1016/j.envint.2023.108273, 2023.

Zhu, S., Sartelet, K. N., Healy, R. M., and Wenger, J. C.: Simulation of particle diversity and mixing state over Greater Paris: a model-measurement inter-comparison, Faraday Discuss., 189, 547–566, https://doi.org/10.1039/C5FD00175G, 2016.